Can chemical short-range order be transformed into a practical alloy-engineering tool?

Zongrui Pei[1,*], Yilun Gong[2,3], Prashant Singh[4], Yue Li[3,5], Fritz Körmann[3,6,7], Qingge Xie[5], Kun Wang[8], Xiaoxiang Wu[9], Sai Mu[10], Michael C. Gao[11], Peter K. Liaw[12], Yang Tong[13], Fan Zhang[14], Yang Wang[15], Rui Li[12]

[1]New York University, New York, NY 10003, USA
[2] University of Oxford, Parks Road, Oxford OX1 3PH, UK
[3]Max Planck Institute for Sustainable Materials, Düsseldorf, 40237, Germany
[4]Ames National Laboratory, U.S. Department of Energy, Iowa State University, Ames, IA 50011, USA
[5] University of Science and Technology Beijing, Beijing, 100083, China
[6]Institute for Materials Science, University of Stuttgart, Pfaffenwaldring 55, 70569 Stuttgart, Germany
[7]Interdisciplinary Centre for Advanced Materials Simulation, Ruhr-Universität Bochum, 44801 Bochum, Germany
[8] New York State College of Ceramics, Alfred University, Alfred, NY 14802, USA
[9] School of Iron and Steel, Soochow University, Suzhou, 215137, China
[10]Department of Physics and Astronomy, University of South Carolina, Columbia, SC 29208, USA
[11]National Energy Technology Laboratory, 1450 Queen Ave SW, Albany, OR 97321, USA
[12] University of Tennessee, 851 Neyland Drive, Knoxville, TN, 37996, USA
[13] Institute for Advanced Studies in Precision Materials, Yantai University, Yantai, Shandong, 264005, China
[14] School of Materials Science and Engineering, Beijing Institute of Technology, Beijing 100081, China
[15]Pittsburgh Supercomputing Center, Carnegie Mellon University, Pittsburgh, PA 15213, USA
[*]Corresponding author.
E-mail: peizongrui@gmail.com; zp2137@nyu.edu

Chemical short-range order (CSRO) is prevalent across many metals and alloys and has recently gained particular attention in concentrated alloys. The advent of complex concentrated alloys has spurred renewed interest in understanding and controlling CSRO. Here, we review recent experimental and theoretical progress on CSRO, highlighting both advancements and ongoing controversies, particularly regarding its impact on the physical properties of concentrated alloys. For example, a highly debated issue is the effect of CSRO on mechanical strength, which remains unresolved due to limited experimental measurements confined to a narrow annealing-temperature range, even for widely studied alloys like CoCrNi. Evaluation of the CSRO effects on various physical properties is critical to answer a central question: Can CSRO be transformed into a practical alloy-engineering tool? We also identify critical gaps in the experimental and theoretical frameworks to achieve this goal. Despite the extensive study of CSRO, there remains a need for methodologies that enable its practical application in alloy design. We explore potential solutions, emphasizing the promising roles of machine-learning potentials and additive manufacturing in creating novel avenues for CSRO control.

keywords: chemical short-range order; alloy design; materials properties; experiment; simulations

Contents

1 Introduction **2**

2 What is CSRO? **4**
2.1 Does CSRO have a characteristic size? . . . 6
2.2 What are possible references to define CSRO? . . . 7
2.3 How to make CSRO simulations and experiments consistent and comparable? . . . 7

3 Can we accurately characterize or predict them now? **8**
3.1 Experiment . . . 8
3.1.1 Transmission Electron Microscopy . . . 8
3.1.2 Neutron scattering . . . 10
3.1.3 Atom Probe Tomography . . . 13
3.1.4 Best practices . . . 15
3.2 Theory . . . 15
3.2.1 Green function-based method . . . 17
3.2.2 Explicit DFT-Monte Carlo approaches . . . 21
3.2.3 Machine-learning potentials . . . 22
3.2.4 Cluster-expansion and associated methods . . . 22
3.2.5 Strain-energy-corrected cluster expansion . . . 23

4 CSRO and physical properties **25**
4.1 Does CSRO affect mechanical properties? . . . 25
4.2 CSRO and radiation damage . . . 26
4.3 CSRO and hydrogen embrittlement . . . 30
4.4 CSRO and transport properties . . . 30

5 Challenges of transforming CSRO into a useful alloy-design tool **32**
5.1 Experimental challenges in controlling CSRO . . . 33
5.2 Lack of accurate temperature-dependent CSRO data . . . 33
5.3 Lack of practical TTT diagrams . . . 35

6 Opportunities and outlook **35**
6.1 CSRO as part of heterogeneous structures . . . 35
6.2 Additive manufacturing . . . 36
6.3 Machine-learning potentials . . . 36

1 Introduction

Complex concentrated alloys (CCAs) have attracted extensive research effort since 2004 [1, 2, 3, 4]. CCAs are also referred to as multicomponent alloys and multi-principal element alloys [5]; when the

number of components exceeds three, they are also called high-entropy alloys due to their higher configurational entropy compared to that of conventional alloys, such as binary alloys. Among their attractive features, the chemical short-range order (CSRO) and its effects in CCAs and other materials have garnered considerable attention in the materials community [6, 7, 8, 9, 10, 11, 12, 13, 14, 15, 16, 17]. One of the current experimental efforts primarily focuses on characterizing CSROs using methods, such as transmission electron microscopy (TEM), atom probe tomography (APT), and neutron scattering. However, controversies exist due to the resolution limitations of the instruments and multiple possibilities in interpreting the characterizations. Advances in the resolutions of these characterization methods by new technologies are critical. One promising direction for such an effort is to combine these tools with machine-learning techniques. For example, it has been shown that APT combined with machine learning can improve characterization quality [10].

Beyond characterization, experimental efforts need to expand toward fine-tuning CSRO and designing alloys with controllable CSRO. Depending on whether CSRO benefits the desired alloy properties, it can either be promoted or suppressed. Traditional methods offer some control by altering chemical compositions and annealing temperatures. However, CSRO tuning is often guided more by empirical practices than by precise theoretical tools, as CSRO is not yet well integrated into existing ICME (Integrated Computational Materials Engineering) frameworks or phase diagrams. For instance, experimentalists typically rely on experience to optimize CSRO formation, such as extending cooling times based on convenience rather than theoretical predictions. Qualitative guidance, like the Hume-Rothery rules, suggests that significant atomic-size mismatches enhance CSRO due to the structural inhomogeneity that they introduce. Nevertheless, current techniques only reveal CSRO in a sample post-synthesis through methods, such as APT or TEM, which adds significant cost and reduces flexibility in CSRO studies. To advance CSRO research systematically, we must first develop reliable methods to synthesize samples with precisely controlled CSRO, enabling a more efficient and flexible approach to understanding and utilizing CSRO in alloy design.

Ideally, theoretical methods, including simulations and modeling, should guide experimental efforts. However, it is currently primarily used to provide post hoc explanations of observed phenomena, rather than as a predictive or guiding tool. For example, it is used to rationalize the K-state phenomenon [9] and to explain the wavy dislocation patterns [14]. The challenge, then, is how to transform theory into a practical guiding tool. The physical quantities that we need to achieve this include accurate temperature-dependent CSRO; then, we will know at what temperature to anneal samples to obtain the desired CSRO. The temperature-dependent CSRO has not been accurately calculated with affordable effort. A few studies focusing on CSRO do not predict it due to the inefficiency of the methods. Temperature-dependent stacking fault energy (SFE) is another critical quantity in alloy design but is also challenging to calculate. For example, in one recent study, the qualitative trend of SFE as a function of temperature was investigated and attributed to varying CSRO, which can explain the width of stacking faults in experiments [18]. However, their method, which is based on density functional theory calculations and Monte Carlo simulations, cannot give a reliable temperature-dependent SFE. The latter requires sufficient sampling of configurations, which is too expensive for first-principles methods [16]. If we can calculate the diffusion rate or coefficients, we can estimate the time to approach the equilibrium CSRO states. We can accurately model interactions for the targeted systems and run simulations for a sufficiently long time to calculate the so-called time-temperature-transformation (TTT) curve for CSRO. In that case, we do

not need the trial-and-error design style to include CSRO. Nonetheless, some of the information remains inaccessible using current methods. We will discuss the gaps and the efforts required to fill them.

Due to the limitations mentioned above and beyond, controversies exist regarding the effects of CSRO on various physical properties. For example, there is controversy over the impact of CSRO on mechanical properties in face-centered-cubic CCAs, such as yield stress. For instance, Zhang *et al.* observed a substantial difference in yield stress between two groups of carefully prepared CoCrNi samples with different levels of CSRO. Li *et al* observed strongly wavy dislocation lines [14], which, according to the theory of solute-solution strengthening, indicates an additional strengthening on top of the intrinsic yield stress. Chen *et al.* found CSRO enhances both the strength and ductility simultaneously [15]. However, a few studies draw different conclusions. For example, Yin *et al.* carefully selected a few experimental measurements of the yield stresses of CoCrNi [13, 19, 20, 21, 22, 23] and subtracted the Hall-Petch effect to check the impact of CSRO. Based on the data, they argued that there is no noticeable difference. We have resolved this issue in a previous study [17], which demonstrates the importance of accurate theoretical methods. Here, we will discuss techniques and physical quantities that are missing to help resolve controversies alike.

Despite significant research efforts, the field remains rapidly evolving with ongoing debates surrounding several aspects: (i) the definition of CSRO (whether confined to a limited region or more extensive), (ii) its formation mechanisms (via heat treatment and chemical doping), (iii) characterization methods, (iv) computational modeling, (v) its impact on mechanical and other physical properties, and (vi) its potential as a practical and controllable tool in alloy design. Some challenges are inherent to the nature of CSRO (weaker than long-range order); others are related to the nature of CCAs (solid solutions involving similar chemicals with weaker diffraction and contrast). Some are due to technical limitations, either in simulations or experiments. We will discuss the issues mentioned above and beyond, their origins, and offer our insights into their solutions. We intend to clarify these points and discuss the current state of the art in this field.

2 What is CSRO?

There are various definitions of CSRO based on mathematical or physical concepts like probability, pair-correlation function, structural motifs, local coordination polyhedra, radial distribution function, mutual information, entropy, and graph-based features. Some are mathematically equivalent, and others are not. One of the most frequently used definitions is the Warren–Cowley short-range order parameters, illustrated in Figure 1, where the corresponding long-range order parameter is also shown for comparison. The nearest-neighbor CSRO is typically used to characterize chemical ordering; it can be defined between any atomic sites, ranging from nearest neighbors to infinitely distant neighbors.

Given its importance, we describe the Warren-Cowley definition of CSRO here first. Generally, any configuration can be defined by occupation variables ξ. If a site i is occupied by atom type μ, $\xi^i_\mu = 1$; otherwise $\xi^i_\mu = 0$. Obviously, for a configuration $\{\xi^i_\mu\}$, $\sum_\mu \xi^i_\mu = 1$ and $\langle \xi^i_\mu \rangle = c_\mu$ (concentration of element μ). The Warren-Cowley CSRO is defined as

$$\alpha^{i,j}_{\mu,\nu} = q^{i,j}_{\mu,\nu}/c_\mu(\delta_{\mu,\nu} - c_\nu) \tag{1}$$

in real space, where $q^{i,j}_{\mu,\nu} = \langle \xi^i_\mu \xi^j_\nu \rangle - \langle \xi^i_\mu \rangle \langle \xi^j_\nu \rangle$. Instead of $\alpha^{i,j}_{\mu,\nu}$, we find the renormalized CSRO parameter

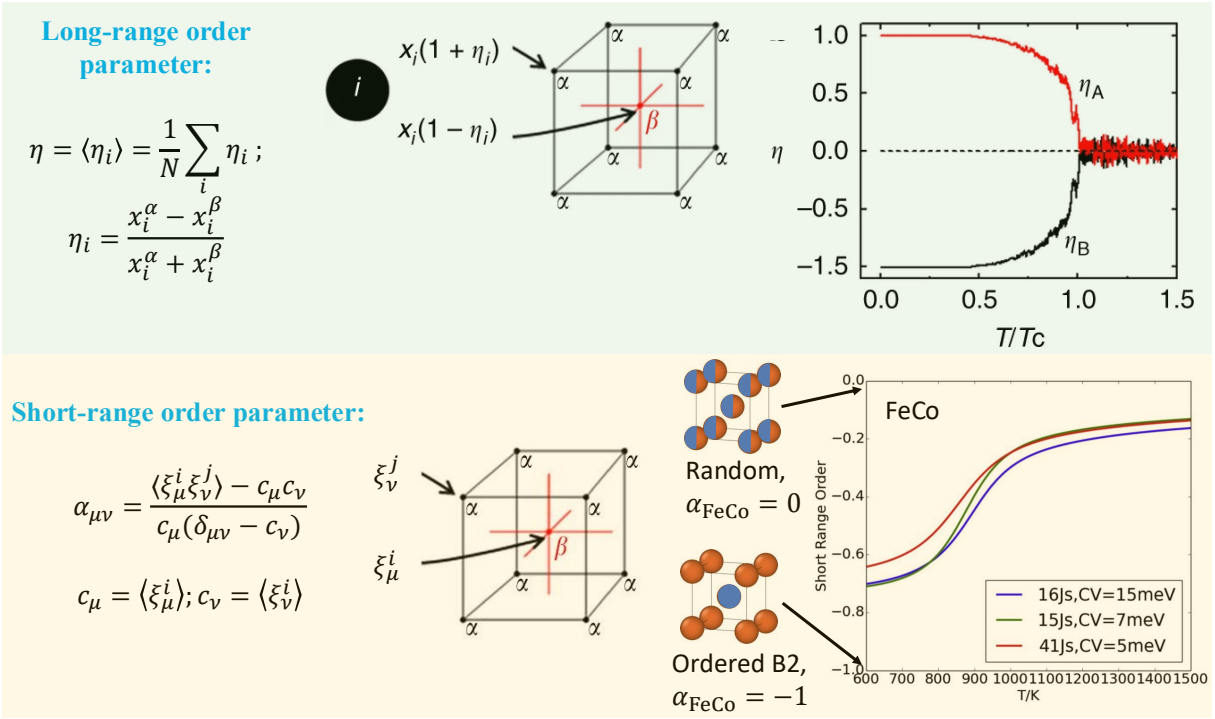


Figure 1: The definition of long-range order and short-range order parameters. The BCC lattice is used to define both types of order parameters, where α, β represent two types of sublattices. The random and ordered B2 structures of FeCo are used to demonstrate the two extreme cases for CSRO. Some notations: N-system size; ξ_μ^i-site occupation. This figure is adapted from Ref.[24, 25].

$Q^{i,j}_{\mu,\nu} = (q^{i,j}_{\mu,\nu} + c_\mu c_\nu)/c_\mu$ is a physically transparent alternative [17]. The quantity $Q^{i,j}_{\mu,\nu}$ conveys the same information as the Warren-Cowley one but has an explicit physical meaning, i.e., averaged site occupations for atoms. We still call it the CSRO parameter in this context. Usually, the CSRO of the nearest neighbors is used. CSRO parameters beyond the nearest neighbors have similar behavior and do not offer much new information if the concern is the order-disorder transition and the degree of CSRO (see Figure 5(b) of Ref. [26]).

The term "chemical short-range order" includes at least three pieces of information: (i) First, it is about the disorder. At zero Kelvin, atoms form an ordered ground state. At finite temperatures, the disorder is unavoidable in samples on a macro-scale, no matter how small the probability is. Usually, if the phase state is dominated by ordered phases, we still consider the material to be in an ordered state; otherwise, ordered materials like line compounds and intermetallics only exist in theory. (ii) Second, it is about atoms of different chemical species. In a solid state, the same atoms cannot introduce configurational entropy, which is the source of chemical disorder. Atoms of the same species can also form different phases, like liquid and gas, but they cannot coexist at a wide temperature range except at transition temperatures. Therefore, atoms of the same species cannot introduce short-range order. (iii) Third, it has a space range, not a long-range, but a short range. But how short? Typically, the spatial extent of CSRO is limited to the first few coordination shells [27], although there is no clear or universally accepted definition. What we know is that, in an ideal random solid solution, the CSRO disappears since there is no correlation between atoms of any species at any distance. In another extreme case, when long-range order exists, the atomic positions become deterministic due to the maximized atomic correlations. Conventionally, the atomic pattern in the long-range setting is repeated with perfect periodicity across the entire crystal, while CSRO is assumed to spread across to only a few atomic distances (nanoscale), e.g., 1st or 2nd nearest-neighbor shells, and sometimes up to the 3rd or 4th, depending on temperature, system, and interactions.

To obtain reliable CSRO information, it is vital to examine the cutoff for interactions. The influence of interatomic interactions on CSRO depends on the specific material system and the methods used to calculate the interactions. Different systems (e.g., FeCo [24] and Ni-Cr alloys [28]) and various methods (e.g., CE [24] and generalized perturbation method [28]) can yield very different values, which must be tested and confirmed for theirto be convergent. If the CSRO in reciprocal space is needed, the cutoff used to calculate it must be tested as well. The reciprocal CSRO is usually defined as

$$\alpha_{\mu,\nu}(\boldsymbol{k}) = \sum_{n_{\boldsymbol{R}}} \alpha^{i,j}_{\mu,\nu}(\boldsymbol{R}) e^{2\pi i \boldsymbol{k}\boldsymbol{R}}, \tag{2}$$

where $n_{\boldsymbol{R}}$ is the cutoff of the real-space CSRO. For a specific material and chosen energy-calculation method, it is also important to test convergence in the calculation of the reciprocal CSRO.

2.1 Does CSRO have a characteristic size?

Does CSRO have a characteristic size, or is it homogeneous beyond the nano-scale? It is inherently inhomogeneous at the atomic scale — otherwise, it would not exist [29]. According to the definition of CSRO parameters, even subtle chemical fluctuations can introduce measurable ordering [30]. Therefore, it seems unreasonable to claim CSRO in a system based on non-zero CSRO parameters. For example,

when ordered clusters with a definite size are embedded into homogeneous solid solutions, CSRO parameters are non-zero, but such configurations are typically not classified as CSRO [31]. The term "local chemical ordering" is sometimes used to describe ordered clusters, which cannot be replaced with CSRO. Notably, when these clusters grow larger in size, they are often treated as second phases. From this point of view, we do not support the view that CSRO has a well-defined size, although we acknowledge that some authors may argue otherwise. Rather, we emphasize that CSRO lacks clear or featured spatial boundaries. In thermodynamic equilibrium, these seemingly independent clusters connect to form huge clusters, thereby minimizing energy [32].

2.2 What are possible references to define CSRO?

Is CSRO defined using the ordered state or the random state as the reference? At finite temperatures, atoms prefer to escape the lattice sites that they originally occupied at zero Kelvin due to thermal fluctuation. Some level of disorder is introduced. Theoretically, we can never approach zero Kelvin, i.e., some level of disorder or randomness always exists in real materials. In very high-temperature regions that are right below the melting temperature, alloys usually exist in solid-solution phases. When chemical elements are similar in atomic size, electronegativity, and the preference for crystal structures in pure materials, solid solutions are sometimes treated as ideal or regular solid solutions, where atoms are arranged at random. Both idealized models assume that atoms randomly occupy any lattice sites without preference. Differently, the ideal solid solutions assume no enthalpy of mixing, while the latter assumes that the enthalpy $\Omega x_A x_B$ is proportional to the concentrations multiplied by an interaction parameter Ω. High temperature provides sufficient energy to overcome the preference.

Both the ordered phase (assume only one ordered phase is formed) and solid solutions are homogeneous on a large scale since the probability of finding a chemical species is proportional to its concentration. Theoretically, both states are straightforward to describe. They can serve as references to define CSRO parameters that describe the intermediate states. Suppose G is a state function of the system, and x represents CSRO. When a system is close to the ordered state, we find $G(x) \approx G(1) + G'(1)(x-1) + \frac{G''(1)}{2!}(x-1)^2 + O((x-1)^2)$; when it is close to complete randomness, $G(x) \approx G(0) + G'(0)x + \frac{G''(0)}{2!}x^2 + O(x^2)$. The simplicity explains why dedicated analytical models exist to describe states near ideal solid solutions and near ideal ordered states, for which even analytical solutions are available [33].

2.3 How to make CSRO simulations and experiments consistent and comparable?

The states between the ordered and random phases are complex, and atoms are in a partially ordered state, a condition common to many materials. Theoretically, it is easy to define CSRO: we check the averaged probability of the neighboring atoms for a targeted atom, and if it equals its concentration, we say there is no CSRO. Here, we did not define the volume used to calculate CSRO, which is critical. In small volumes, we will always have CSRO, although we may say that if it only slightly deviates from the concentration, there is no CSRO. In a huge volume close to the thermodynamic limit, the value can approach the true CSRO, when there is no secondary phase. CSRO is affected by sample volumes in measurements or calculations, which are usually larger in experiments than in simulations. *Here comes another question: How can we make the simulation and experiment for CSRO consistent and*

comparable? Currently, our choice of volume in either an experiment or simulation is from a practical point of view. In theoretical calculations, limited by computational methods and resources, researchers use the largest possible supercells to model CSRO. In the electron microscopy experiment, the CSRO is characterized by diffraction patterns that utilize the local part of the sample interacting with electrons. The guiding principle is that we first need to identify all the individual phase regions and calculate CSRO for each of the separate phases. It may not be sensible to calculate CSRO for the whole sample if multiple phases exist. We also need to check the effect of system size on the calculated CSRO and ensure it is controllable and negligible.

3 Can we accurately characterize or predict them now?

3.1 Experiment

Experimental method to measure CSRO either relies on the contrast or the difference in atoms interacting with light particles (electrons or neutrons), which is not significant, or suffer from the loss of atoms (atom probe tomography). We need to improve current instruments to augment the experimental signals to obtain high-quality data to characterize CSRO, or use machine-learning methods to distill high-quality information from noisy data.

3.1.1 Transmission Electron Microscopy

Transmission electron microscopy (TEM) is one of the most widely used experimental methods to study order-disorder phenomena [35] and CSRO [11, 34, 36, 8, 37, 38, 39, 40]. For example, Zhang *et al.* used TEM to study CSRO in CoCrNi and found particles of approximately 1 nm distributed in the FCC matrix [11]. If the boundaries of the so-called particles are vague or uncertain, then it is more appropriate to use other terminology instead of the word "particle" to avoid potential confusion. If the boundaries are clear and certain, the claimed CSRO may be more suitably described by local chemical ordering. The diffraction mode of energy-filtered TEM identified additional diffraction patterns besides those belonging to FCC, as seen in Figure 2 (a-b). They concluded that these patterns were due to CSRO. In another medium-entropy alloy, CoCrV, Chen *et al.* provided S/TEM evidence of the CSRO, including a diffraction pattern on the appropriate zone axis, atomic-resolution imaging, and chemical mapping [34]. Here, CSRO is confirmed with diffuse diffraction disk at the position corresponding to $\frac{1}{2}\{\bar{3}11\}$. The CSRO region corresponds to a size of 0.6$\sim$1 nm, as shown in Figure 2 (c-h). Although additional diffuse diffraction patterns are commonly used for identifying CSRO, we need to consider whether the diffraction patterns are indeed due to CSRO.

In a recent study, Walsh *et al.* found that not all extra electron reflections are necessarily related to CSRO [8], and the diffuse intensities may originate from planar defects or due to weaker dynamical effects. In another study, through combined experimental TEM and multislice simulations, Walsh *et al.* further demonstrated that these features largely arise from thermal displacement scattering (correlated atomic vibrations) and static displacement scattering (lattice distortions due to atomic size/charge differences), which reproduce observed diffuse intensities in key zone axes ([111] and [112]) [41]. Other contributors include incommensurate surface terminations (causing sharp superlattice intensities in the [111] zone axis), weaker dynamical scattering artifacts (e.g., higher-order Laue zone diffraction, or HOLZ

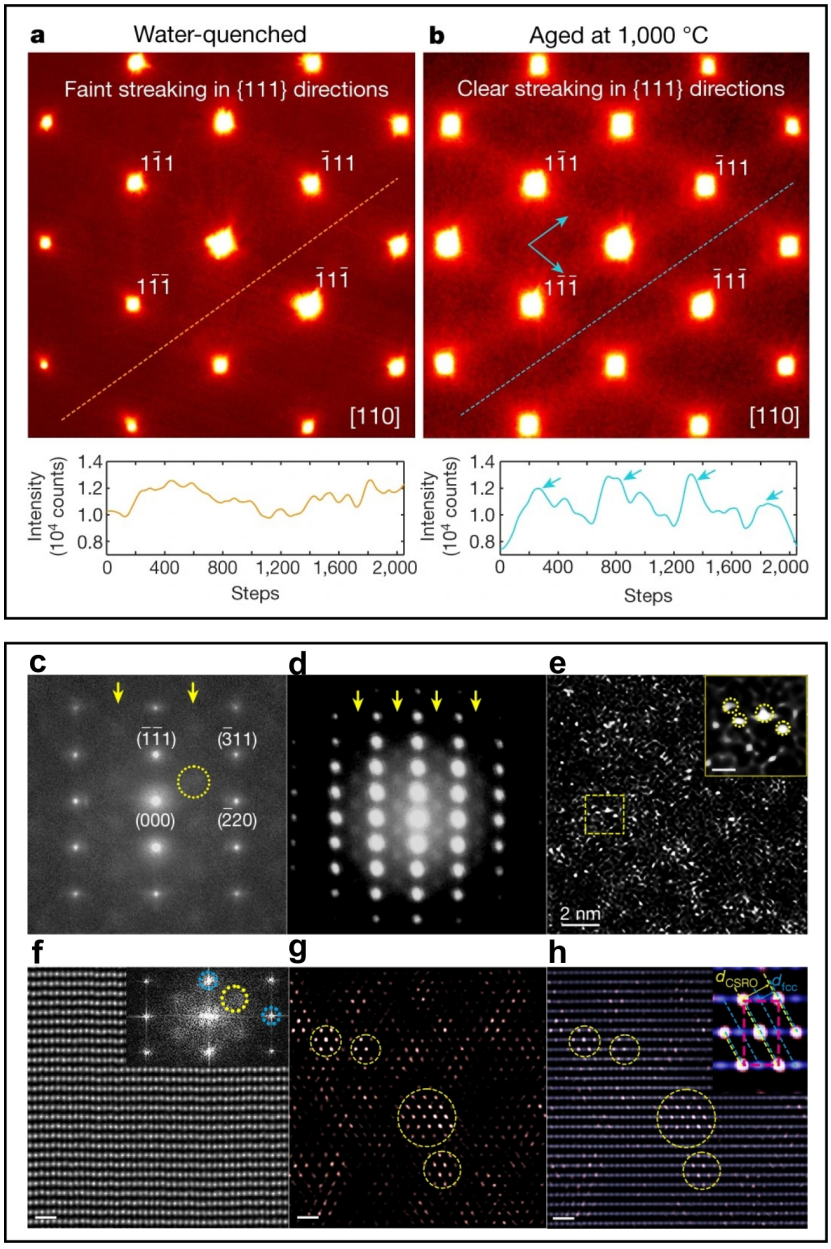


Figure 2: Observation of CSRO under transmission electron microscopy. **a-b**: CSRO in CoCrNi, adopted from Ref.[11]; **c-h**: CSRO in CoCrV, adopted from Ref. [34]. Here, the signal of CSRO is indicated by arrows for both CoCrNi and CoCrV in diffraction patterns.

diffraction in short), and occasionally planar defects (e.g., stacking faults). Critically, CSRO has a negligible effect on ambient-temperature diffraction patterns, challenging the widespread interpretation that diffuse scattering directly signifies chemical ordering in these alloys. The multiple possible origins of the diffraction pattern indicate that CSRO could be one, and further research efforts are needed to clarify the issue [37]. This controversy arises partly due to the limited capability of TEM.

3.1.2 Neutron scattering

Unlike in conventional alloys, the different atomic species in CCAs are thought to be randomly distributed. Their strengths may not be attributed to the anomalous levels of strains [42], and other mechanisms need to be explored to explain the variation in strength. Besides the atomic radius and the shear modulus of the individual elements, the CSRO may play an essential role in the strength of nominally disordered CCAs [43]. Between two extreme cases—(1) random solid solutions driven by entropic effects and (2) solid solutions with long-range ordered structures formed due to favorable enthalpy values—CSRO structures represent an intermediate state, formed by increasing enthalpy through the formation of certain atomic bonds while simultaneously losing a certain degree of entropy. CSRO typically involves the nearest neighbors of an atom, and it indicates any elemental distribution that deviates from the average on a local-length scale. The local-atomic structure can be indirectly revealed using diffraction-based techniques (neutron and X-ray) and X-ray absorption measurements [44].

The choice between the X-ray and neutron diffraction for CSRO studies depends on the alloy elements. The scattering strength is roughly proportional to the atomic number for X-ray measurements. An alloy comprised of chemical elements with different atomic numbers has a sharp scattering contrast. However, the chemical elements with a close atomic number would be impractical for X-ray measurements. Also, X-rays have difficulty detecting light chemical elements. In addition, the immersed volume for the X-ray measurement is much smaller than that of the neutron due to lower penetration thickness. Therefore, the crystallite size in the sample prepared for X-ray measurements must be as small as possible. For neutrons, the scattering length does not have any periodic trend. Then, neutron diffraction gives a different contrast from that of X-ray. In some cases, the study of Cu_3Au, as an example, neutron diffraction is not possible because of the almost identical neutron-scattering lengths [45].

Employing X-ray/neutron diffraction, the total scattering in the analysis of CSRO provides valuable insight into the atomic structure. When atoms scatter X-rays or neutrons, the direction change depends on the relative positions of atoms, which can reflect the arrangement of the atoms. A total scattering experiment gives information on both (1) the long-range crystallographic order by analyzing the Bragg peaks and (2) the short-range fluctuations. The former indicates the lattice parameters. The latter provides not only average positions of atoms but also CSRO through the diffuse scattering. The diffuse scattering is across the entire diffraction pattern and forms the central part of the background for powder diffraction. Diffuse scattering contains the information on the atomic structure or the arrangement of the average positions. The spatial distribution of atoms relative to one another in a system is usually represented by the pair distribution function (PDF) spectrum, as shown in Figure 3. The PDF indicates the probability of finding an atom at a distance, r, from another atom. A peak in the PDF indicates the average distance of one atom relative to another, which signals local ordering. Valleys suggest that atoms are less likely to be found. For example, the first peak represents the average nearest-neighbor distance. Its width depends on the distribution of the inter-atomic distance that is controlled by the number and scattering

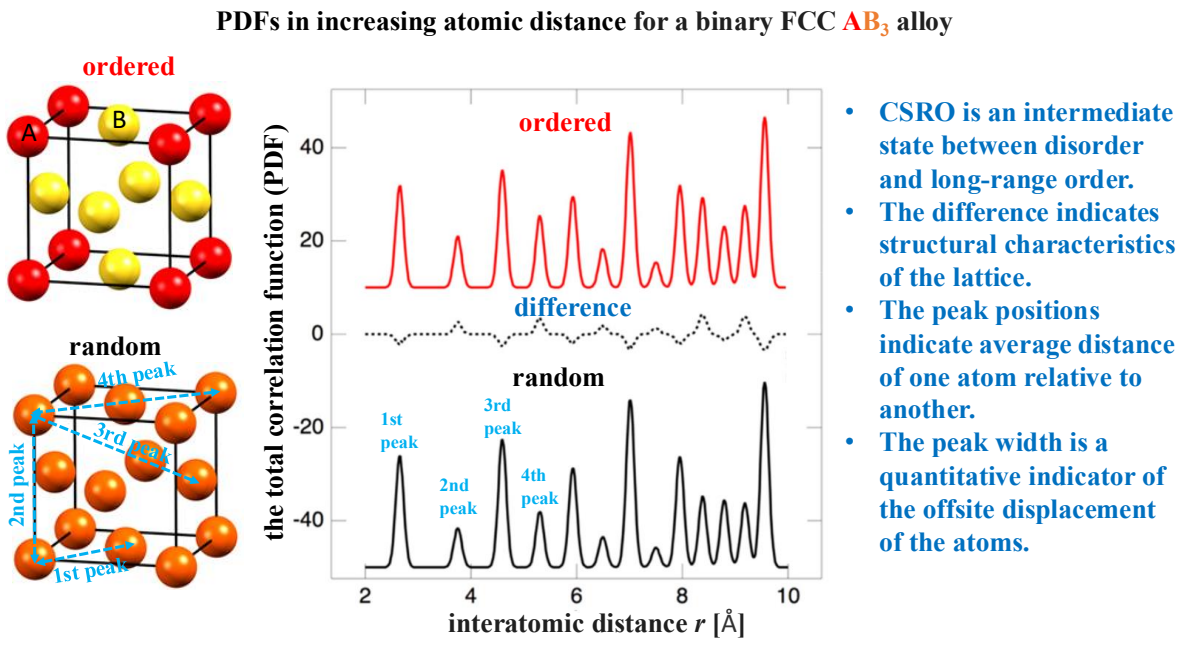


Figure 3: The atomistic models combined with pair-distribution functions (PDFs) provide the quantitative structural information about the types of CSRO. The figure is adopted from Ref. [45].

length of the related atoms. The peak area is a function of the number and type of correlations at that distance. Therefore, the PDF gives a weighted histogram of the distribution of distances between atoms. For the AB_3 binary FCC alloy shown in Figure 3, there may be a change in the average interatomic distances of the different pairs of atoms. Larger atoms may lead to lattice expansion and peak shifts. The resulting lattice strain can induce an increase in the peak width. The AB and BB average distances may be different from the AA bond length. Also, the width controlled by the distribution of the interatomic distances may change in comparison with that of the pure monatomic case. By identifying which peaks change and the extent of the change, the type of order in a system can be revealed. To explore CSRO, a systematic method for the analysis of short-range order was proposed as follows [45]: 1. The measured sample should be free of the crystallographic texture to maximize the number of illuminated crystallites. 2. Measuring the total scattering, preferably using neutron or synchrotron-based X-ray due to their small wavelengths. 3. By analyzing the total scattering data, suitable atomistic models representing both long-range and short-range order are produced using either simulation methods (for example, the reverse Monte Carlo algorithm) or refinement techniques. 4. An iterative procedure is employed to obtain a statistically good agreement between the information content of pair distribution functions and that obtained by Fourier transformation of the experimentally measured total scattering data, where various types and degrees of CSRO were explored. CSRO can be identified through (a) Warren-Cowley distributions to obtain the type and magnitude of order, (b) the Clapp configuration enhancement factor to determine the local arrangement of atoms, and (c) Degradation pathways to identify the key structural motifs and related long-range order structures.

The diffuse scattering due to CSRO may become superlattice peaks when a long-range order is established: CSRO peak positions are at which the superlattice peaks will form, and the breadth of CSRO peaks is several times that of the Bragg peaks. For β-CuZn alloy at room temperature, as an example, it forms a long-range order structure. With temperature increasing and at the critical temperature Tc, the structure is disordered. Such an order-disorder transformation can occur in any alloy, regardless of its crystal structure. For X-ray diffuse scattering, Cu and Zn are close neighbors in the periodic table that feature similar X-ray scattering factors. Then, X-ray diffuse scattering is not possible to detect the order-disorder transformation. Neutron diffraction is a feasible technique. The average neutron- scattering lengths differ appreciably for these pairs of atoms. This difference can be enhanced by using isotopes [46].

The CSRO was often investigated in austenitic Ni-based alloys. NiFeCr alloys retain a disordered FCC structure from the melt to liquid-helium temperature. By analyzing diffusely scattered intensity from the single crystal, the first experimental evidence of ordering between Ni and Cr atoms in stainless-steel-type alloys was obtained [47]. In a second example, the atomic redistribution under irradiation in austenitic NiFeCr alloys has been investigated by diffuse neutron scattering. The changes in CSRO induced by irradiation could be attributed mainly to the formation of Ni-Cr pairs [48]. For a CoCrNi alloy, Co and Ni are highly similar in atomic sizes, electronic structures, shear moduli, and many other aspects. To detect the possible structural distortion of the CoCrNi alloy, a total scattering measurement was conducted with neutron diffraction for the polycrystal samples. For neutron total scattering, the PDF spectrum was well refined with a randomly distributed FCC structure model over the whole range. A Rietveld refinement of the neutron PDF spectrum of the CoCrNi yields a Debye-Waller (DW) factor that is noticeably larger than that of pure Ni at room temperature. However, a PDF analysis cannot distin-

guish the bond length and vibrations of pairs between different atomic species because of the very similar atomic sizes and comparable neutron-scattering properties. To obtain the detailed local-structure information, the extended X-ray absorption fine structure (EXAFS) technique was employed. In comparison with PDF, which renders the information for a large number of coordination shells, EXAFS provides the first couple of shells. The DW factors derived from EXAFS indicate the relative change in the bond length. Smaller DW factors of Cr-Ni and Cr-Co suggest that there exists a CSRO in which Cr atoms tend to separate from each other, and more Ni(Co)-Cr pairs exist [49].

3.1.3 Atom Probe Tomography

Atom probe tomography (APT) has emerged as a powerful tool for analyzing CSRO at the atomic scale. Due to its high spatial resolution and elemental sensitivity, APT enables the three-dimensional reconstruction of materials with near-atomic precision. However, inherent challenges, such as anisotropic spatial resolution and imperfect detection efficiency, impose limitations on its ability to characterize CSRO accurately. To overcome these constraints, researchers have explored data-driven approaches, particularly leveraging machine learning (ML) to enhance the analytical capabilities of APT.

A recent development in this direction was introduced by He et al. [7], who proposed a data-driven framework to quantify CSRO in CoCrNi alloys. Their approach accounts for APT's spatial resolution errors and detection inefficiencies by establishing threshold values for identifying regions where atomistic neighborhood information remains reliable. By applying correction factors, this method improves the accuracy of CSRO analysis, offering a more precise representation of atomic arrangements.

In a parallel effort, Li *et al.* [51] introduced a machine-learning-assisted APT strategy, termed ML-APT, which employs convolutional neural networks (CNNs) to enable tomographic imaging of CSRO in various engineering materials. The methodology begins with the generation of simulated spatial distribution maps (SDMs), which serve as a training dataset for CNNs to recognize ordered and disordered structures. Experimental SDMs are then extracted from APT datasets and processed using the trained models to reveal chemical and crystallographic details of CSRO. This technique has successfully been used to investigate long-standing questions in Fe-based alloys, such as the K-state behavior in Fe-Al and Fe-Ga systems. The ML-APT framework enabled the identification of unexpected B2-CSRO in Fe-Al alloys and modified DO_3-CSRO in Fe-Ga alloys, offering more profound insights into their structural characteristics.

While ML-APT has proven effective, it initially required prior knowledge of potential CSRO configurations, limiting its applicability in complex alloy systems. To address this, Li et al. [10] further extended the ML-APT framework to analyze CSRO in CoCrNi alloys without predefined CSRO structures. By systematically evaluating elemental pair correlations along different crystallographic directions, they deduced the presence of $L1_2$/DO_{22}- and $L1_1$-CSRO configurations in CoCrNi alloys [Figure 4]. The fruitful quantitative information on these CSRO structures, such as their number density, size, and morphology, can be obtained. This advancement pushed the resolution of CSRO domain recognition below 1 nm, expanding APT's capability to study chemical ordering at the nanoscale, even in compositionally complex alloys [52].

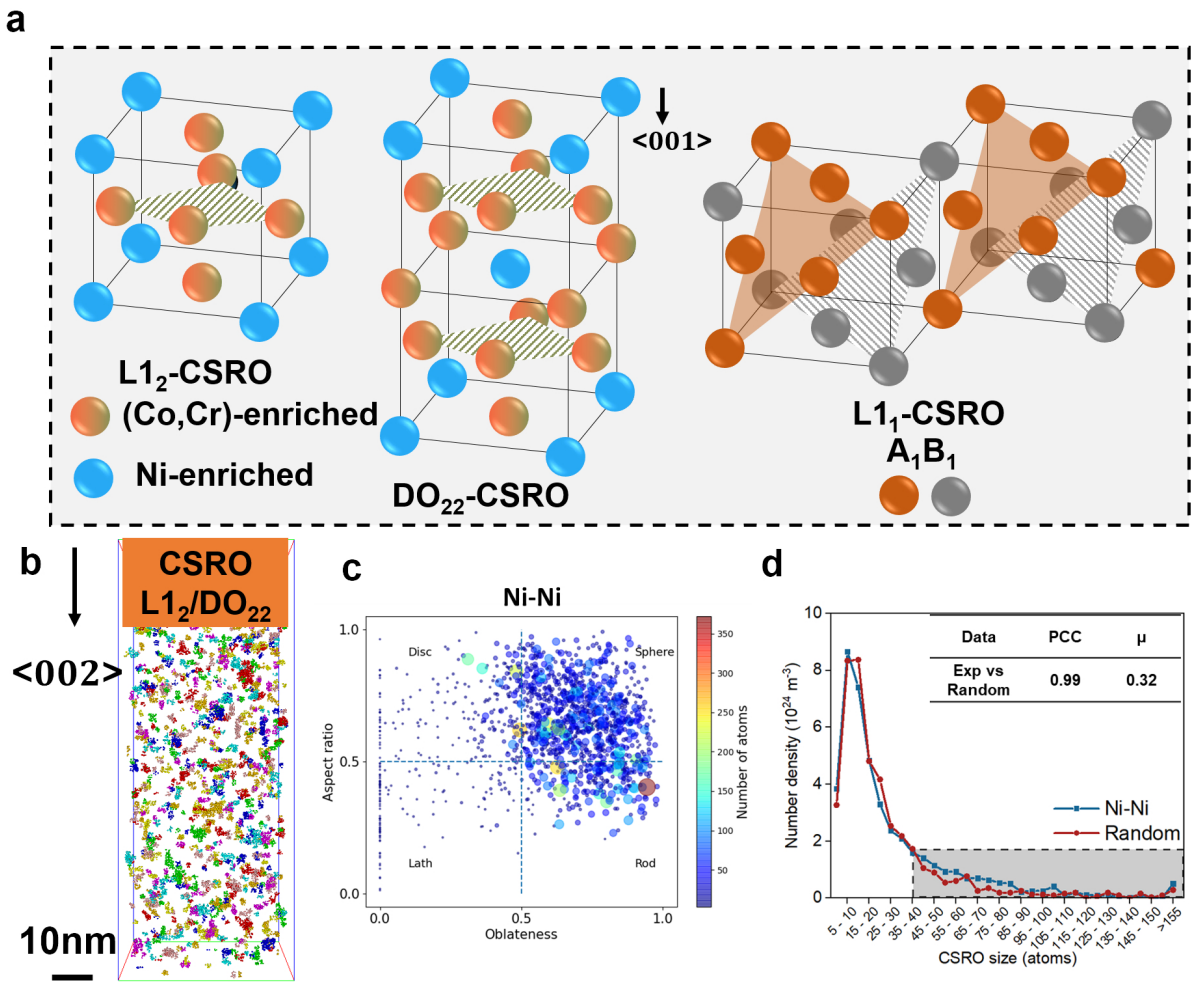


Figure 4: Multiple types of CSRO domains in 3D in an annealed CoCrNi alloy obtained using the proposed machine-learning APT approach[10, 50]. **a**, Experimentally derived CSRO configurations and elemental site occupancies. **b**, Three-dimensional map of the $L1_2/DO_{22}$-type CSROs. **c-d**, The corresponding morphology and size distributions.

3.1.4 Best practices

Although the experimental techniques can all be used, their limitations are apparent, as we have discussed above. For example, TEM use the diffraction patterns additional to a reference (ordered or random system) to identify CSRO, which may have multiple origins (e.g., planar defects and weaker dynamic effects); APT provides three-dimensional real-space reconstructed structure on atomic scale, where chemical ordering can be directly observed but suffers from anisotropic spatial resolution and imperfect detection efficiency; neutron scattering provides PDF information that reveal CSRO through the derivations from ideal structures, which suffers from peak overlap (peaks from multiple atom pairs often overlap) and resolution limits.

Due to the limitations, we recommend the best practices to interpret CSRO, which include: (i) perform multiple characterizations for different parts of a single samples or multiple samples to obtain statistically reliable results; (ii) utilize multiple experimental techniques for cross-validation, e.g., the usage of both TEM and APT to characterize the same sample, which can significantly increase the reliability of results; (iii) adopt theoretical simulations to validate experimental observations, e.g., use MC simulations to directly calculate the CSRO and compare it with the experimental measurements; (iv) avoid exaggeration when the data is insufficient to draw reliable conclusions.

3.2 Theory

We summarize a few theoretical methods used to calculate CSRO in Figure 5. CSRO is a statistical property that can be calculated from either Monte-Carlo/molecular dynamics simulations or analytical approximations. Such calculations require numerous repetitive energetic calculations to obtain CSROs close to the equilibrium states, which is impractical to use computationally expensive first-principles methods like density functional theory explicitly. Directly using the first-principles method to drive Monte Carlo or molecular dynamics is theoretically possible, but this method only provides a qualitative trend of CSRO, not an accurate CSRO at a given temperature. Therefore, various computationally efficient surrogate models have been developed, which rely on first-principles methods to generate data to determine surrogate models. Then, these surrogate models are utilized in Monte-Carlo or molecular dynamics simulations to calculate CSRO.

Typical surrogate models include (i) traditional empirical potentials, e.g., embedded atom methods (or EAM in short), (ii) machine-learning potentials that have attracted extensive attention recently, (iii) cluster-expansion-type models, such as the original rigid lattice model [53], atomic cluster expansion (ACE) [54], the moment tensor potential (MTP) [55], etc. From a general viewpoint, some recent cluster-expansion-type potentials, such as ACE and MTP, can also be grouped with machine-learning potentials, as they are formulated in a variational form with unknown parameters that can be optimized, similar to training a machine-learning model. Typical machine-learning potentials include those based on deep neural networks and Gaussian approximation potentials (GAP) [56], among others. In contrast to the aforementioned surrogate models, Green function-based Korringa-Kohn-Rostoker (KKR) methods [57, 58], such as the cluster-averaged coherent potential approximation (CPA) method [59] and the locally self-consistent multiple scattering (LSMS) method [60], offer a direct and ab initio link between CSRO and the electronic density within the framework of DFT. The KKR methods, depending on specific implementations, can yield CSRO-related information without sorting to statistical simulations.

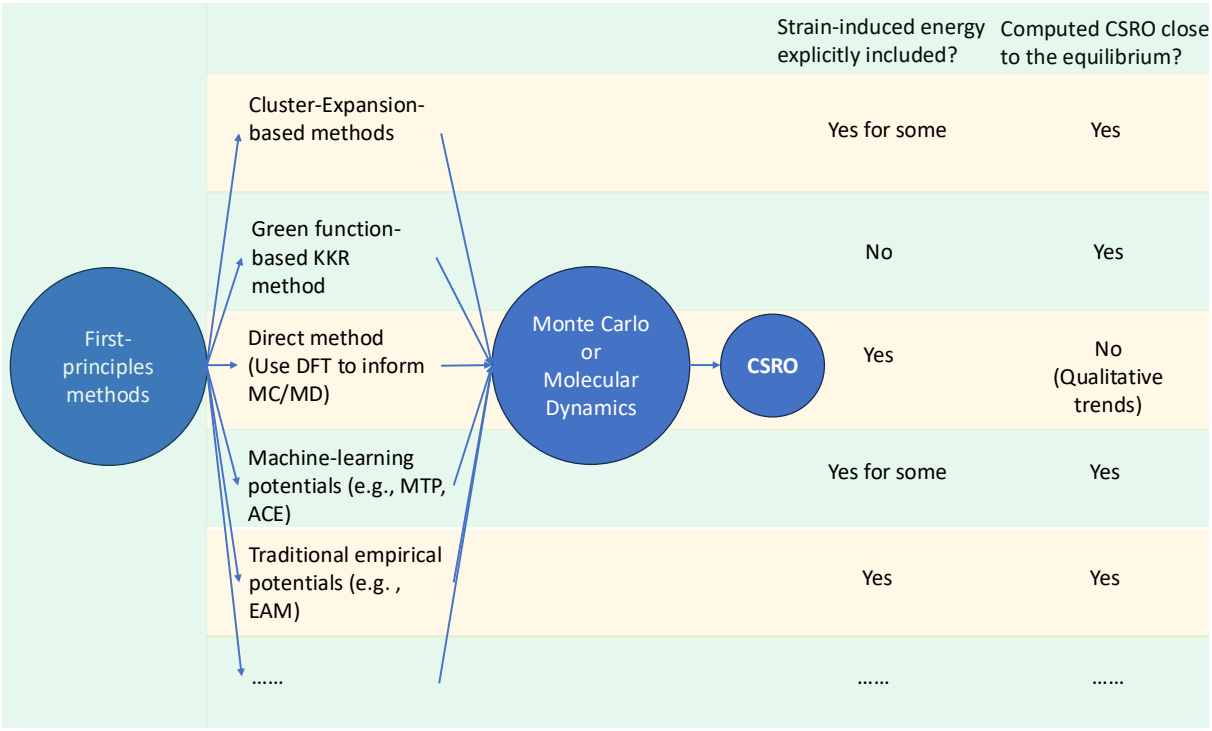


Figure 5: Summary of theoretical methods for CSRO calculations. We also comment on whether the strain-induced energy is included and whether the computed CSRO is close to the equilibrium.

However, they can also be used to inform surrogate models for statistical simulations [61].

We briefly comment on two features of the individual methods in Figure 5, i.e., (i) whether the strain-induced energy is included and (ii) whether the computed CSRO is close to the equilibrium. Cluster-expansion-type surrogate models typically do not explicitly include strain-induced energy in their computed total energies. However, the strain-induced contribution can be added, assisted by the elastic Green function [17]. Green function-based KKR methods are theoretically capable of incorporating lattice distortions. For instance, the LSMS method can achieve this via a supercell approach, while the KKR-CPA method can employ an alloy-analogy model, which involves averaging over a discrete set of displacements specifically chosen to reproduce the thermal root mean square average displacement at a given temperature [62]. Many machine-learning interatomic potentials allow relaxation of atomic positions, such as GAP, MTP, ACE, etc. This feature is similar to traditional empirical potentials. However, some on-site machine learning potentials, such as the low-rank potentials developed in [63], can only implicitly consider the strain-induced energy but cannot explicitly include this energy contribution by allowing atoms to relax. The traditional empirical potentials, primarily based on the EAM method, enable atomic relaxation and explicitly include the strain-induced energy. Limited by computational efficiency, the direct method that uses DFT to inform statistical simulations is impractical for calculating CSRO close to the equilibrium. It can yield a CSRO trend but cannot accurately determine the CSRO at a given temperature. The other methods included in the figures, albeit with lower accuracy, can calculate CSRO at a temperature close to the equilibrium. More details beyond these two features are elaborated on in the section below.

3.2.1 Green function-based method

Diffuse scattering intensities in alloys—measured using x-ray, electron, or neutron techniques — provide critical insights into ordering tendencies, especially in the solid-solution phase above structural transformation temperatures, where most processing occurs. However, despite their technological relevance, multicomponent alloys present significant experimental and theoretical challenges. As a result, most studies have focused on binary or pseudo-binary systems, with only limited exploration of true multicomponent behavior. This raises key questions: How can diffuse scattering be interpreted in complex alloys, and how can theory accurately predict their ordering tendencies?

The Green function-based linear-response method, developed within the Korringa-Kohn-Rostoker coherent potential approximation (KKR-CPA) framework, provides a robust first-principles approach—via the concentration wave formalism—for calculating CSRO in these multicomponent disordered alloys [64]. As we have discussed in Sec. 3.1, CSRO is experimentally accessible by diffuse scattering techniques (X-ray, electron, or neutron), which enable the extraction of the Warren–Cowley CSRO parameters, $\alpha_{\mu\nu}(\mathbf{k})$ at the wavevector, $\mathbf{k}$. These parameters represent normalized pair-correlation probabilities. For multicomponent alloys, diffuse scattering intensities are typically expressed in Laue units,[64, 26, 65, 66, 67, 68, 69, 70, 71, 72, 73, 74, 75] taking the form:

$$I(\mathbf{k}) = \sum_{\mu,\nu} c_\mu(\delta_{\mu\nu} - c_\nu)\left[f_\mu - f_\nu\right]^2 \alpha_{\mu\nu}(\mathbf{k})\,, \tag{3}$$

where f_μ is the atomic form factor of species, μ, and c_μ is its composition. Only off-diagonal $\alpha_{\mu\nu}$ terms contribute to scattering if there is sufficient contrast ($f_\mu \neq f_\nu$). In binary A–B systems, for instance, the

single off-diagonal $\alpha_{\rm AB}(\mathbf{k})$ is directly measurable, with diagonal components recoverable via sum rules derived from the optical theorem. The interpretation is straightforward: in regions where an A atom is absent, a B atom is preferentially located in an ordering pattern determined by $\mathbf{k}$. The normalized pair correlations, $\alpha^{ij}_{\mu\nu}(\mathbf{k})$, are defined via $\alpha^{ij}_{\mu\nu}(\mathbf{k}) = \frac{q^{ij}_{\mu\nu}(\mathbf{k})}{c_\mu(\delta_{\mu\nu}-c_\nu)}$, where the pair-correlation function is $q^{ij}_{\mu\nu}(\mathbf{k}) = \langle\xi^i_\mu\xi^j_\nu\rangle - \langle\xi^i_\mu\rangle\langle\xi^j_\nu\rangle$ and ξ^i_μ is the site occupation variable. These quantities in reciprocal space have the same mathematical forms as their real-space counterparts.

Linear-Response Formalism: Using linear-response theory, CSRO parameters are computed from second-order concentration variations in the alloy grand potential [64]. The relevant quantity is the chemical stability matrix $S^{(2)}_{\mu\nu}(\mathbf{k})$, given by:

$$\left[q^{-1}(\mathbf{k})\right]_{\mu\nu} = \left[\frac{\delta_{\mu\nu}}{c_\mu} + \frac{1}{c_N}\right] - \beta S^{(2)}_{\mu\nu}(\mathbf{k}), \tag{4}$$

where $\beta = (k_B T)^{-1}$ and the indices μ, ν run over the $N-1$ independent species. At the spinodal temperature, $T_{\rm sp}$, the lowest eigenvalue of $[q^{-1}(\mathbf{k})]$ vanishes, signifying the onset of ordering. The corresponding eigenvector identifies the ordering mode and chemical species involved. In the linear-response theory, $\mathrm{S}^{(2)}_{\mu\nu}(\mathbf{k})$ is the second variation of the alloy Grand Potential with respect to composition fluctuations, evaluated in the high-temperature disordered phase.[64, 65] That is, expanding the interacting electronic part of the free-energy in a functional Taylor's series relative to the disordered alloy, we find[70, 72, 73, 74, 75] that

$$\begin{aligned}
\Delta F(\{c^i_\mu\}) &= F(\{c^i_\mu\}) - F(\{\bar{c}_\mu\}) \\
&= \frac{1}{2}\sum_{\mu\nu,ij} \Delta c^{\dagger i}_\mu \frac{\delta^2 F}{\delta c^{\dagger i}_\mu \delta c^j_\nu}|_{\{c_\mu\}} \Delta c^j_\nu \\
&\approx \frac{1}{2}\sum_{\mu\nu}\int_{BZ} d\mathbf{k}\, \Delta c^\dagger_\mu(\mathbf{k}) S^{(2)}_{\mu\nu}(\mathbf{k}) \Delta c_\nu(\mathbf{k}),
\end{aligned} \tag{5}$$

and where the first variation is zero by symmetry of the disordered state. The Brilliouin zone (BZ) integral is over that of the solid-solution's Bravais lattice, where the fluctuations, $c^i_\mu - \bar{c}_\mu$ (i.e., Fourier wave $\Delta c_\mu(\mathbf{k})$) happen. The total alloy free energy, $F = F_0 + F_{\rm int}$, can be written as the sum of non-interacting, F_0, and interacting, $F_{\rm int}$, contributions, where F_0 is related to point entropy (S_{pt}) [i.e., $TS_{pt} = -k_{\rm B}T\sum c^{\rm i}_\mu \ln c^{\rm i}_\mu$], and $F_{\rm int}$ comes from electronic structure (ion-ion, band-energy, double-counting and exchange-correlation). $S^{(2)}_{\mu\nu}(\mathbf{k})$ is determined from $F_{\rm int}$ in the solid-solution phase. The above formalism, implemented using KKR-CPA Green's function methods[64, 65, 68], allows for the evaluation of $\alpha_{\mu\nu}(\mathbf{k})$ in terms of electronic structure effects such as band-filling, hybridization, Fermi surface nesting, and van Hove states.

If evaluated in the homogeneous state, $\alpha_{\mu\nu}(\mathbf{k})$ is an approximation to the state with actual CSRO, and it can be calculated with the KKR-CPA linear-response framework. The ability to compute CSRO parameters, $\alpha_{\mu\nu}(\mathbf{k})$, and associated instabilities from electronic structure enables fundamental insights into chemical ordering, which are crucial for the design of CCAs and other disordered materials.

We provide one each examples of refractory CCAs, i.e., BCC TaNbMoW (Figure 6a-c) [65] and a medium-entropy alloy (MEA), i.e., FCC CoCrNi (Figure 6d-g) [76], that reveal how electronic mecha-

nisms, such as Fermi-surface nesting or thermodynamics, govern the onset and nature of atomic CSRO in chemically complex alloys.

Notably, in the BCC TaNbMoW, CSRO above the spinodal temperature T_{sp} in Figure 6a is dominated by Ta–Mo bainry interactions, with a prominent peak at an incommensurate wavevector, $\mathbf{k}o \approx \frac{1}{2}(\mathrm{P}-\mathrm{H})$, exceeding that at Γ. This suggests long-period modulations driven by electronic instabilities, consistent with the behavior of $S^{(2)}_{\mathrm{TaMo}}(\mathbf{k};T)$. Real-space pair interactions, particularly for the BCC TaNbMoW, show oscillations up to the 30th shell in Figure 6b, with amplitudes between -1 and $+1$ mRy-signatures of Fermi-surface effects. The (001) Fermi surface projection confirms nesting near $\mathbf{q}_s = \frac{3}{4}(\Gamma - \mathrm{H})$, Figure 6b, correlating with diffuse scattering peaks. These features establish that the observed CSRO leads to experimentally observed clustering, which originates from flat electronic dispersion near the Fermi level. The (001)-projected Fermi surface convolution in TaNbMoW clearly shows nesting features at $\mathbf{q}_s = \frac{3}{4}(\Gamma - \mathrm{H})$ in Figure 6c, which correlates directly with diffuse intensities in Figure 6a. Greens's function-based linear-response theory could capture these intricate details as it considers all ranges of $k-$space interaction, which are handled on par with one another [64]. In contrast, recent results from the generalized perturbation method (a real space method) suggested commensurate CSRO with a B2+B32 mixed groundstate, from an unknown origin with Fermi-surface effects improperly dismissed [77]. The difference between the two methods is related to the relative numerics of the generalized perturbation method (GPM) and the real-space method (over 70 shells arising from embedding pairs of atoms at varying ranges) [65].

The FCC CoCrNi alloy is another tricky example where CSRO reveals distinct ordering tendencies and structural properties [11, 78, 79, 80, 76, 81]. In Figure 6d, the CSRO is plotted along high-symmetry directions in the Brillouin zone at $1.15T_{\mathrm{sp}}$ ($T_{\mathrm{sp}} = 300$ K), which shows a dominant peak near the X-point, with values exceeding 2.0 Laue, indicating a strong predisposition toward $\mathrm{L1_2}$-type ordering. The competing tendencies between Ni-Co, Ni-Cr, and Co-Cr pairs are evident, as each shows different wavevector preferences and CSRO amplitudes. This internal competition contributes to complex chemical ordering patterns. Temperature-dependent CSRO plot for Ni-Co pairs in Figure 6e shows a clear reduction in ordering amplitude with a change in temperature from 1,473 K to 350 K. At 350 K, CSRO is still well-defined and concentrated near X (001) and W (1,1/2,0) points, but by 1,473 K the correlations are significantly suppressed, approaching a nearly random alloy. This thermodynamic evolution underscores the entropy-driven disordering process and also reflects the small energy scales associated with ordering in this system—on the order of a few milli-Rydbergs.

Formation energies in Figure 6f provide insight into the relative stability of potential ordering phases of the CoCrNi MEA. The disordered FCC phase is taken as a reference, while several ordering candidates such as $\mathrm{D0_{22}}$, $\mathrm{MoPt_2}$, and $\mathrm{L1_2}$ lie 5–7 mRy lower in energy. The CSRO-based prediction, marked in red, lies closest to $\mathrm{D0_{22}}$, indicating that the observed short-range correlations may be precursors to this phase, even in the absence of full long-range order. Neutron-diffraction patterns from aged samples further validate these predictions. The neutron-diffraction image in Figure 6g shows diffuse intensity at non-Bragg positions (e.g., 012 and 021), which matches with the FCC + $\mathrm{L1_2}$ CSRO scenario predicted theoretically. The correspondence between accurate CSRO predictions using a linear-response theory and neutron data affirms the role of electronic-structure-informed first-principles methods in explaining and predicting ordering behavior in multicomponent alloys, even in regimes weakly dominated by short-range correlations, as exemplified in FCC CoCrNi.

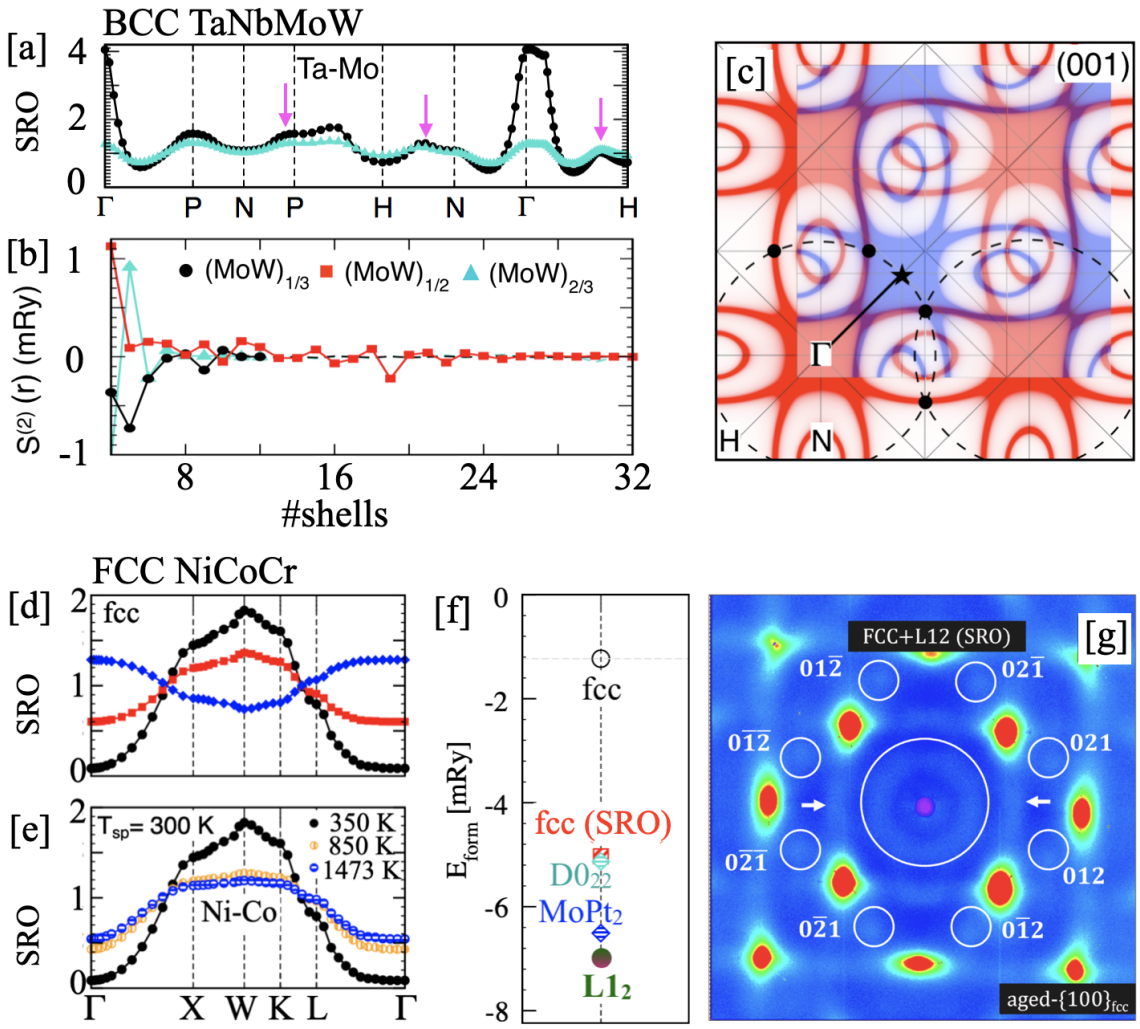


Figure 6: Chemical short-range order (CSRO) in the BCC TaNbMoW and FCC CoCrNi alloys. CSRO was calculated using an electronic structure method based on Green's functions. **a**, Momentum-resolved CSRO for the BCC TaNbMoW showing dominant incommensurate ordering near $\mathbf{k}_o \approx \frac{1}{2}$(P–H), driven by Ta–Mo correlations. **b**, Real-space pair interactions, $S^{(2)}(r)$, for Mo–W pairs in various compositions, highlighting long-ranged oscillatory behavior due to Fermi-surface nesting. **c**, (001)-projected Fermi surface convolution in TaNbMoW showing nesting features at $\mathbf{q}_s = \frac{3}{4}(\Gamma - \mathrm{H})$ that correlate with diffuse intensities. **d**, CSRO in FCC CoCrNi at $T_{\mathrm{sp}} = 300$ K, indicating strong Ni–Co-driven ordering tendencies around X and W points. **e**, Temperature dependence of CSRO from 350 K to 1,473 K, showing thermally induced disordering. **f**, Formation energies of various ordered structures relative to the disordered FCC phase; the red circle shows the energy of the CSRO-predicted structure. **g**, Neutron-diffraction pattern from aged CoCrNi showing diffuse peaks consistent with $L1_2$-like CSRO, validating the theoretical predictions.

Advantages, drawbacks, and future directions: The Green function-based approach provides a powerful *ab initio* framework for modeling atomic interactions in multicomponent alloys without relying on empirical parameters. At the core of the approach is a first-principles, electronic-structure-based method for predicting CSRO. By employing a linear-response formulation within the coherent potential approximation, this approach captures the thermodynamic fluctuations around the disordered state, making it well-suited for complex and high-entropy systems. This method predicts both the sign and magnitude of atomic interactions, offering insights into mixing behavior and phase stability. Additionally, it can identify dominant ordering vectors in reciprocal space, enabling the construction of free energy landscapes and the prediction of phase transitions such as spinodal decomposition or ordering tendencies.

In multicomponent alloys, this Green's function-based approach provides a complete understanding of ordering tendencies requiring not only identifying unstable wavevectors but also determining the polarization of the associated ordering waves. These polarizations, which reflect the directional characteristics of atomic correlations, can be obtained from CSRO−both theoretically and experimentally−and, notably, through analysis of diffuse-scattering intensities, an insight that has been largely overlooked.

While the theory operates within a mean-field approximation, it accounts for various competing electronic and entropic mechanisms on equal footing. This is especially relevant in metallic alloys, where key energetic differences are often just a few milli-Rydbergs, making even a 10% error in calculated transition temperatures remarkably accurate−sometimes performing even better. When CSRO predicts a low-temperature ordered phase, the method also reveals the electronic driving forces behind the transformation[82]. However, it does not capture effects such as statistical fluctuations beyond mean field or cluster-level entropy, which can lead to first-order transitions absent in CSRO. In such cases, more advanced statistical approaches like Monte Carlo simulations may be employed, provided the relevant energetics can be computed with sufficient relative accuracy.

3.2.2 Explicit DFT-Monte Carlo approaches

First-principles methods, such as density functional theory (DFT), can be directly used to drive molecular dynamics (MD) or Monte Carlo (MC) simulations. Joint efforts of these methods can calculate the CSRO at different temperatures. Given the computational cost of DFT, MC based on it can only provide a qualitative trend of CSRO rather than a temperature-resolved CSRO [18]. Theoretically, it can be used to calculate temperature-dependent CSRO, but it requires an impractically long time to achieve equilibrium. The hybrid MC/MD methods have been developed to accelerate simulations toward equilibrium. However, obtaining the equilibrium CSRO is not straightforward. Nonetheless, we can still obtain qualitative information on CSRO from such methods.

The temperature-dependent CSRO provides ordering information at thermodynamic equilibrium. Theoretically, this thermal trend cannot be achieved; it can only be approached asymptotically. In practice, the system is treated as being in thermodynamic equilibrium after a certain amount of time, when the CSRO is very close to theory. To understand the kinetic process of CSRO evolution and estimate the time required to approach thermodynamic equilibrium, we need MD or kinetic Monte Carlo (kMC). The kMC method explicitly includes kinetic rates proportional to the Boltzmann factors, calculated from the energy barriers. The advantage of kMC is that it accelerates diffusion and can be used to model processes on longer timescales than MD. The kMC method was recently used to study the kinetics of multi-principal element alloys based on energy barriers computed from machine-learning models [83, 84].

3.2.3 Machine-learning potentials

Given the computational costs of direct DFT-based Monte Carlo simulations, machine-learning (ML) interatomic potentials are increasingly used to explore CSRO in materials. There are two types of these potentials: off-lattice and on-lattice potentials, each with strengths and limitations. An overview of these approaches can be found in [16, 85], where typical ML potentials, such as the neural network potential within the Behler-Parrinello framework [86], were summarized. On-lattice potentials can incorporate local relaxation effects if a unique mapping to the host lattice remains, similar to the cluster expansion Hamiltonian technique discussed below. One particularly efficient on-lattice ML potential is the low-rank potential developed in [63], which has been applied to CSRO calculations in various complex alloys, such as NbMoTaW [87] and CrCoNi [88, 10, 89]. Typically, these on-lattice potentials require several hundred total energy DFT calculations to perform reliable Monte Carlo simulations.

ML interatomic potentials (MLIPs) not confined to specific lattice structures are more commonly employed. These potentials allow one to perform, e.g., coupled Monte Carlo and molecular dynamics simulations, including thermal vibrations and self-consistent lattice expansion into CSRO calculations. Among others, the atomic cluster expansion [54] and moment tensor potentials [55] are frequently used. These ML potentials also include forces and stresses, but their construction often necessitates thousands of DFT calculations. Once constructed, these ML potentials can be used to investigate, e.g., the impact of CSRO on extended defects, e.g., in NbMoTaW [12]. For CrCoNi, MTPs have also been utilized to study CSRO [90].

However, magnetism, which can significantly influence CSRO (see, e.g., [91, 89]), poses a considerable challenge for ML potentials [92]. Machine-learning interatomic potentials that explicitly account for magnetic degrees of freedom are still in their early stages of development, see e.g., [93, 94]. Main reasons are the complexity and computational demands of generating the necessary, often non-collinear spin training data (often requiring spin-constrained DFT calculations). Complementary efforts include the preprocessing of DFT data to simulate various magnetic scenarios, e.g., for CrCoNi [89], or to incorporate magnetism in a simplified "Ising-like" manner [95, 96]. These methods provide practical solutions as long as the challenges of training more advanced "magnetic" MLIPs remain.

3.2.4 Cluster-expansion and associated methods

The cluster-expansion (CE) method employs parametrized Hamiltonians to calculate the total energy of an arbitrary configuration, σ [53, 24], i.e.,

$$E(\sigma) = \sum_{\alpha} J_\alpha \phi_\alpha(\{s_i\}^N), \alpha = 0, 1, 2, \ldots \tag{6}$$

where $\phi_\alpha(\{s_i\}^N)$ represents the product of the occupation variables, s_i in a cluster, α, and J_α is the effective interaction parameter for the cluster, α. In a N-component alloy, if N is an odd number, $m = (N-1)/2$, $s_i = -m, \ldots, -1, 0, 1, \ldots, m$; if N is an even number, $m = N/2$, $s_i = -m, \ldots, -1, 1, \ldots, m$. For example, for the CoCrNi medium-entropy alloy, $N = 3$, so $m = -1, 0$, and 1. The accuracy of total energies can be improved systematically by adding more terms, thereby including more clusters [53]. The Hamiltonians are theoretically exact when considering all sub-clusters.

The method was used in predicting the ordering transition temperature of the body-centered-cubic (BCC) FeCo alloy [24], face-centered-cubic (FCC) medium-entropy alloys to study the order-disorder

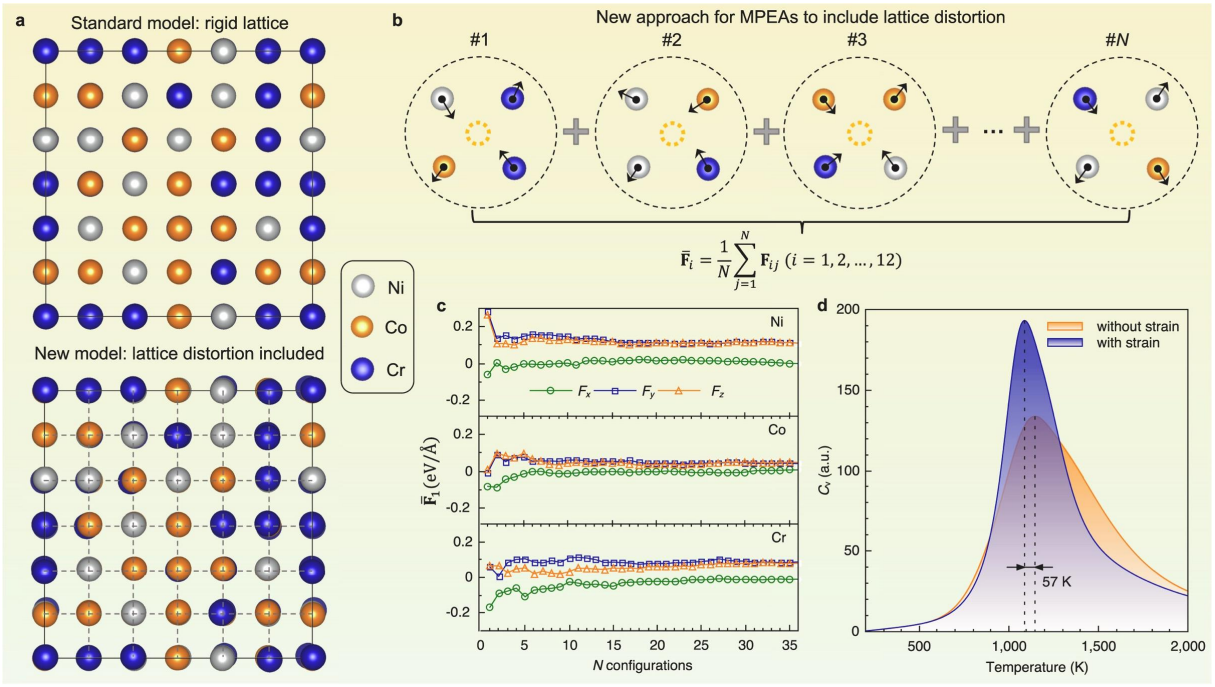


Figure 7: Including strain-induced energy in the cluster-expansion method. We calculate the strain-induced energies, V^{si}, using DFT and employ the elastic Green function to transform them from real space to reciprocal space and then back to real space. Then, we map the energies to the Chebyshev polynomials, which are used as the expansion basis sets. **a**, The rigid model and new model with lattice distortion included. **b**, New approach to include lattice distortion through averaged Kanzaki forces. **c**, Averaged Kanzaki forces on a representative first-nearest neighbor atom induced by a Ni, Co, or Cr atom as a function of the number of configurations. **d**, The specific heat calculated w/o strain correction. This figure is adapted from Ref. [17].

transition [9, 17], and BCC CCAs to study the interstitial cluster formation [97]. A few variants of the methods have been constantly developed in the spirit of the powerful expansion idea, such as the so-called eCE that constructs multicomponent cluster expansions with machine-learning and chemical embedding [98], the CELL method – a Python package for cluster expansion with a focus on complex alloys [99], and ACE that has been introduced above [54].

3.2.5 Strain-energy-corrected cluster expansion

The core idea of cluster expansion (CE) is to partition the total energy of a system into an infinite series of contributions from small clusters, starting from one-body clusters, two-body clusters, three-body clusters, etc. [53]. The mathematical tool to implement this idea is Chebyshev polynomials, which are an orthogonal basis. Usually, a cutoff of the size and diameter of the clusters is exerted when the error is sufficiently small. The original CE method is based on a rigid lattice, meaning that the lattice distortion effect at individual atoms is not explicitly included but implicitly embraced in the energy-structure data

used to fit the CE Hamiltonian. Pei and colleagues used the rigid-lattice CE model to study the statistics of CoCrNi and checked the validity of a few assumptions on pseudo-binary entropy [9]. Recently, they developed a new method that can explicitly consider the local distortion based on the lattice Green function [17]. They used DFT to calculate the total energy and forces at each atomic site, which were utilized to fit a Green function in reciprocal space. Then, the Green function was inverse-Fourier-transformed into real space, which yielded the interaction parameters purely due to local strain. These interaction parameters were further mapped into the coefficients of the orthogonal Chebyshev polynomials, which could then be added directly to the coefficient of CE. Assisted by this new method, they obtained a strain-corrected Hamiltonian for use in Monte Carlo simulations. Compared to the rigid lattice model, the latest model improves the agreement of the transition temperature with experimental measurements.

We briefly describe the essential details of the method here to facilitate our discussion later. The strain-induced interaction is computed using the microscopic elasticity theory (Figure 7), i.e.,

$$V_{mn}^{\mathrm{si}}(\mathbf{R}) = 1/N_{\mathrm{q}} \sum_{\mathbf{q}} V_{mn}^{si}(\mathbf{q}) e^{i\mathbf{q}\mathbf{R}}, \tag{7}$$

$$V_{mn}^{\mathrm{si}}(\mathbf{q}) = -\mathbf{F}_m(\mathbf{q})\mathbf{G}(\mathbf{q})\mathbf{F}_n^*(\mathbf{q}) + Q_{mm}\delta_{mn}, \tag{8}$$

where $Q_{mm} = 1/N_{\mathbf{q}} \sum_{\mathbf{q}} \mathbf{F}_m(\mathbf{q})\mathbf{G}(\mathbf{q})\mathbf{F}_m^*(\mathbf{q})$; Q_{mm} is a correction for the self-interaction. $\mathbf{F}_m(\mathbf{q})$ are the Fourier components of the so-called Kanzaki forces [100] induced by a nearby atom, m, which are defined as the equivalent forces on the host lattice atoms that could induce the same lattice distortion generated by atom, m. The superscript (*) denotes matrix transpose. $\mathbf{G}(\mathbf{q})$ are the Fourier transformed lattice Green's function at $\mathbf{q}$ in reciprocal space. $N_{\mathbf{q}}$ is the total number of $\mathbf{q}$ points. In the case of CoCrNi, the six two-body interaction parameters at each $\boldsymbol{R}$ are computed for the corresponding six atom combinations.

The six two-body interaction parameters at each $\mathbf{R}$ are then transformed into the three-parameter representation used by CE methods. More specifically, we choose nine representative structures of the chemical formula, AB_3 and AA (A,B = Co,Cr,Ni) and calculate their strain-induced energies $E_i^{\mathrm{si}}(i = 0, 1, \ldots, 8)$ using only the two-body terms $V_{mn}^{\mathrm{si}}(\mathbf{R})$, we can get nine equations. The quantity, E_i^{si}, is a combination of $V_{mn}^{\mathrm{si}}(\mathbf{R})$ dependent on atomic species, e.g., $E_{\mathrm{AB_3}}^{\mathrm{si}} = \sum_{\mathbf{R}} \sum_{m,n} M_{mn}(\mathbf{R}) V_{mn}^{\mathrm{si}}(\mathbf{R})$ with m, n = A or B, where $M_{mn}(\mathbf{R})$ is the corresponding multiplicity. Since there are only three unknown parameters and nine equations, we use the least-square method to determine the J_α^{si},

$$\min \left(E_i^{\mathrm{si}}(V_{mn}^{\mathrm{si}}) - \sum_{\alpha} m_\alpha J_\alpha^{\mathrm{si}} \langle \Pi_{j\in\alpha} \sigma_j \rangle \right)^2. \tag{9}$$

Here $\langle \Pi_{j\in\alpha} \sigma_j \rangle$ is the averaged pair correlation function for the cluster, α. Convergence tests are performed and show that nine structures are sufficient to obtain reliable interaction parameters. When six or more structures are adopted, the ECIs remain almost unchanged, signaling their convergence [17]. The new interaction parameters after correction are $J_\alpha = J_\alpha^{\mathrm{si}} + J_\alpha^{\mathrm{ch}}$, where J_α^{ch} are the interaction parameters calculated using the rigid lattice gas models without strains.

4 CSRO and physical properties

Our understanding of the CSRO effect on physical properties is generally insufficient due to the lack of data. Experimentally, we require a sufficiently large annealing temperature range that encompasses at least the ordering transition temperatures for a reasonably long period. Given the slow kinetics at low temperatures, we need to measure the CSRO in the annealed sample and check the actual state and temperature of the sample. To this end, we require theoretical guidance on annealing temperature and temperature-dependent CSRO. The theoretical transition temperature helps determine the annealing temperature, and the theoretical CSRO is used to compare with the experimental CSRO, thereby determining the actual energy state and temperature of the sample. Such information also serves as guidance to design better materials.

Currently, accurate information that is missing from the above picture includes the following: (i) accurate temperature-dependent CSRO or phase diagram with CSRO included; (ii) time-temperature-transformation (TTT) diagram that reflects both kinetics and thermodynamics information; such a diagram instructs design of alloys with tuned CSRO; (iii) sufficiently large temperature range of CSRO and tensile tests.

In this section, we will discuss the state-of-the-art research on CSRO concerning a few critical physical properties, along with typical examples.

4.1 Does CSRO affect mechanical properties?

The influence of CSRO on mechanical properties has been an active research topic that attracts extensive attention [101, 102, 103, 104, 17, 105, 106]. The target of these studies is to answer the same question: Does CSRO have a visible effect on mechanical properties, such as yield stresses? Nonetheless, controversial effects were reported in these studies. Some researchers found a substantial influence on yield stresses, while others argued the impact can be ignored. Which is the correct answer, or what is the most widely accepted answer that may convince researchers from both sides? The short answer is that it is still too early to give a clear answer. What we are certain is that it affects some mechanical properties in some materials. Still, we do not know if this is universally true. To fully address this issue, we need more careful experiments in a wide range of diverse systems. Currently, all experiments for CCAs are conducted on limited systems, such as the Cantor alloy, VCoNi, and CoCrNi. Moreover, in these limited samples, such as CoCrNi, only narrow temperature ranges were investigated in which no CSRO has only negligible changes (Figure 8). This feature is the origin of controversy in CoCrNi. To overcome the experimental limitations, simulation can help answer this question.

The CSRO effect on ductility has also received extensive attention [107, 15, 108, 109]. For example, the atomistic simulations of Chen *et al.* suggest that short-range ordering could enhance the ultimate strength and ductility of high-entropy simultaneously in the CCA CoCuFeNiPd [15]. Their simulations show the energetically favorable CSRO leads to a pseudo-composite microstructure in the material, which consists of face-center-cubic-preferred (FCC-preferred) clusters, indifferent clusters, and body-center-cubic-preferred (BCC-preferred) clusters. They suggested that the FCC-preferred clusters serve as hard fillers to enhance the strength, while the BCC-preferred clusters act as soft fillers to increase the ductility. This pseudo-composite microstructure eventually benefits both the ultimate strength and ductility. Unlike the example above, which was performed between 300 K and 1200 K at cryogenic temperatures,

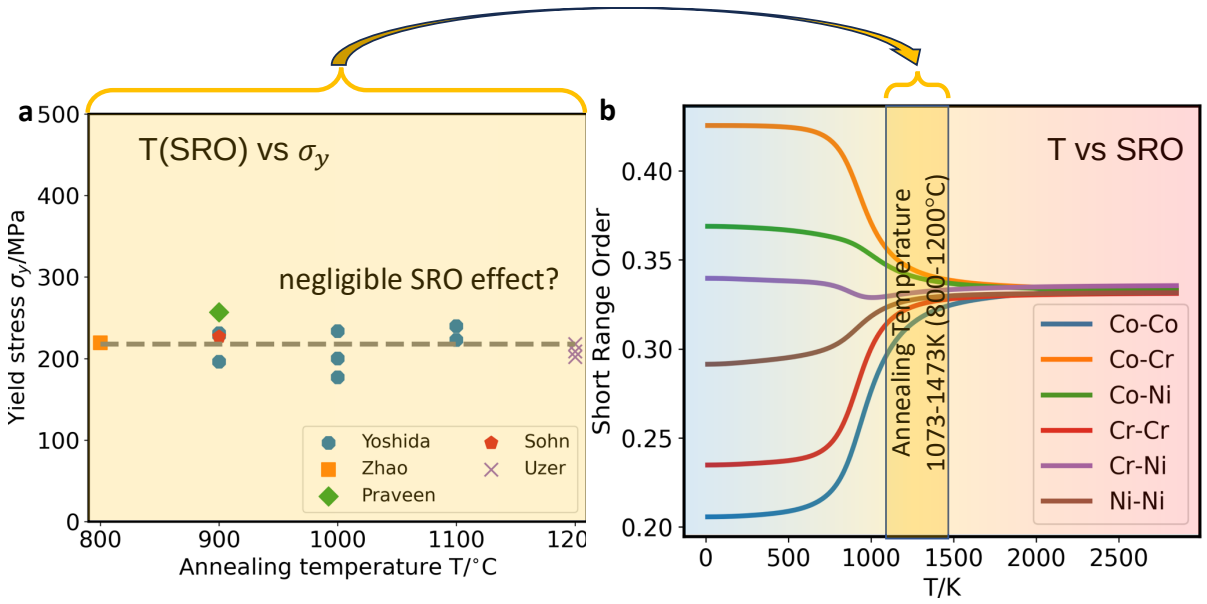


Figure 8: Temperature-dependent chemical short-range order (CSRO) and yield stresses. **a**, yield stresses as a function of annealing temperatures. Data is collected from Yoshida *et al.* [19], Zhao *et al.* [20], Uzer *et al.* [21], Sohn *et al.* [22], Praveen *et al.* [23]. **b**, Temperature dependent CSRO parameters [9, 17]. This figure is adapted from Ref. [17].

Sun and colleagues argued that CSRO enables ultrahigh strength and ductility in Fe49Mn30Co10Cr10N1 alloy [108]. They proposed a combination of a few underlying mechanisms to explain the enhancement. The mechanisms include (i) dense laths composed of the multiscale local chemical ordering (LCO) domains, which contribute to ultrahigh yield strengths, (ii) dislocation cross-slip promoted by LCO, and (iii) deformation-driven transformation and twinning that have been widely found in many materials. In a recent experimental study on fine-grained alloys, Yan and colleagues demonstrated the ductilization of a few 2.6-GPa alloys based on vanadium, cobalt, and nickel [109]. Usually, alloys with such high strengths have limited deformability; however, they identified an extra ductility capability via CSRO near grain boundaries and supranano precipitates. More research efforts are needed to double-check the above-mentioned excellent mechanical properties and the proposed mechanisms.

There are more studies that indicate the important role of CSRO on ductility than not. The statistics suggests CSRO can change ductility substantially, but more research efforts are needed to make a conclusion. We have to put a question mark on the reliability of this statistics, because the data could also be a biased statistics. Researchers prefer to write reports on positive results rather than failures, since it is much easier to publish positive results on top journals rather than negative ones.

4.2 CSRO and radiation damage

Experiments and simulations have demonstrated that CSRO can markedly alter radiation-induced defect formation and evolution. For instance, in the medium-entropy alloy of CrCoNi, irradiation experiments

combined with atomistic simulations revealed that the presence of local chemical order (LCO), developed through thermal aging, effectively delays the formation and growth of defect clusters under irradiation conditions. This enhanced resistance is primarily attributed to the CSRO-induced narrowing of the mobility difference between interstitials and vacancies, which significantly increases recombination efficiency and reduces the accumulation of residual defects, such as stacking-fault tetrahedra and dislocation loops [110]. The diminished radiation effect in multi-principal-element alloys was also discussed by Cao, based on a few representative studies published before 2021 [111]. Possible mechanisms and explanations were proposed based on the CSRO role in point-defect diffusion, defect clusters (dislocation loops and vacancy clusters), and grain boundaries.

Figure 9**a** and **d** show atomic high-angle annular dark-field (HAADF) imaging under the [112] zone axis for the water-quenched CrCoNi [Random Solid Solution (RSS)] and 1,000°C-aged CrCoNi [LCO], respectively. The size and distribution of CSRO are obtained by inverse fast Fourier transform (IFFT) of the diffraction disks (1/2 $\{1\bar{1}3\}$) arising from CSRO, as illustrated in Figure 9 **c** and **f**. Figure 10 presents TEM images of CrCoNi alloys aged at 1,000 °C (RSS) and 1,000 °C (LCO) after various irradiation doses (0.16 to 1.0 dpa). At the low doses of irradiation, such as 0.16 dpa, some defect clusters (white dots) are already present in the water-quenched RSS sample, whereas the corresponding 1,000 °C-aged (LCO) sample is nearly defect-free. With increasing irradiation dose, more defect clusters appear in both samples, although the LCO sample consistently exhibits a lower number density.

In NiCoFeCrMn, it has been shown through advanced electron microscopy that chemical CSRO structures are more prominently developed under irradiation compared to equilibrium conditions. Radiation promotes chemical ordering through the transient thermal spike during displacement cascades and subsequent radiation-enhanced diffusion, significantly increasing the areal fraction of CSRO structures with increasing the irradiation dose and temperature. The radiation-assisted formation of CSRO is considered beneficial for enhancing irradiation resistance, as it plays a role in suppressing defect accumulation and stabilizing the microstructure against radiation-induced degradation [112]. A reactor-relevant neutron campaign on CrFeMnNi (395–579 °C, 6.6 dpa) likewise produced irradiation-enhanced LCO and a parallel drop in the faulted loop density with no swelling, strengthening the causal link between order and tolerance [113].

Atomistic simulations of refractory CCAs, such as HfNbTaTiZr, provide complementary insights. These simulations illustrate how CSRO structures can alter primary radiation-damage mechanisms by inducing cascade splitting into subcascades, thereby dispersing cascade energy and facilitating defect recombination. The presence of CSRO promotes the generation of Frenkel pairs at low defect concentrations but crucially inhibits their accumulation at higher defect concentrations, resulting in superior irradiation resistance compared to their random solid-solution counterparts. Additionally, CSRO has been shown to limit the growth of defect clusters and mitigate the generation of dislocations during irradiation, enhancing material resilience under irradiation conditions [114]. Molecular dynamics (MD) simulations have been conducted to investigate the impact of CSRO on radiation-induced defect behavior in Fe-Ni-Cr alloys. It was discovered that higher CSRO levels reduce defect diffusivity due to trapping effects within Cr-rich domains, significantly altering defect dynamics during radiation exposure. The research notably identified that interstitial clusters become Cr-rich in high-CSRO scenarios, leading to preferential formation and stabilization of interstitial loops near these Cr-rich areas [115].

Moreover, systematic multiscale modeling studies indicate element-dependent CSRO behavior in

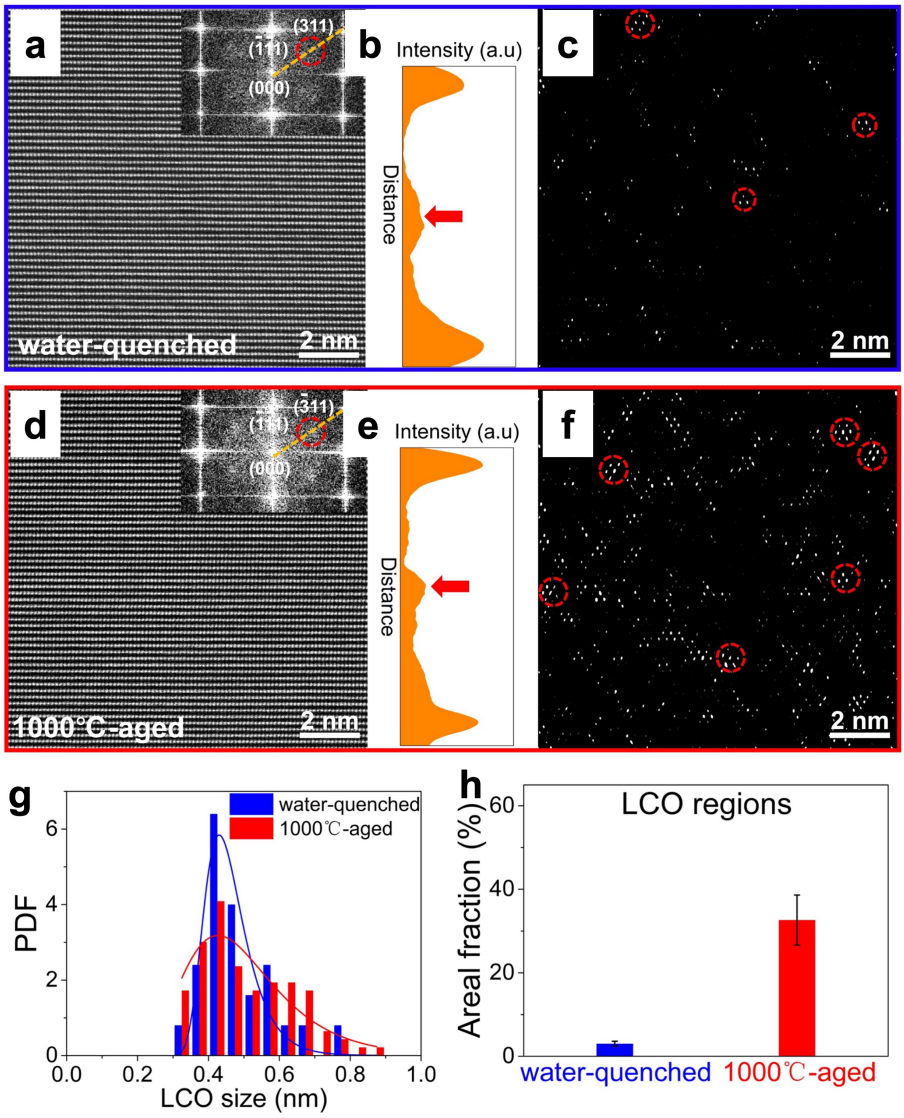


Figure 9: Experimental characterization of LCO. **a**, HAADF-STEM images of the water-quenched CrCoNi alloy in the [112] zone axis; the Inset shows the corresponding FFT, where the red circles indicate diffuse disks at 1/2 $\{\bar{3}11\}$ positions, suggesting the chemically short-range-ordered regions (CSROs) have sizes below one nanometer. **b**, Diffraction intensity along the orange dashed line in panel **a**. The red arrow indicates the extra intensity at 1/2 $\{1\bar{1}3\}$ positions. **c**, IFFT image based on four symmetrical diffraction disks, one of which is highlighted using a dashed circle in panel **a**. Several CSRO regions are marked using red circles. **d-f**, The same characterization as in the Upper panels for the 1,000 °C-aged sample. **g**, Probability density function (PDF) of LCO size (in diameter). **h**, Areal fraction of the LCO regions in the two CrCoNi alloys. This figure is adapted from Ref. [110].

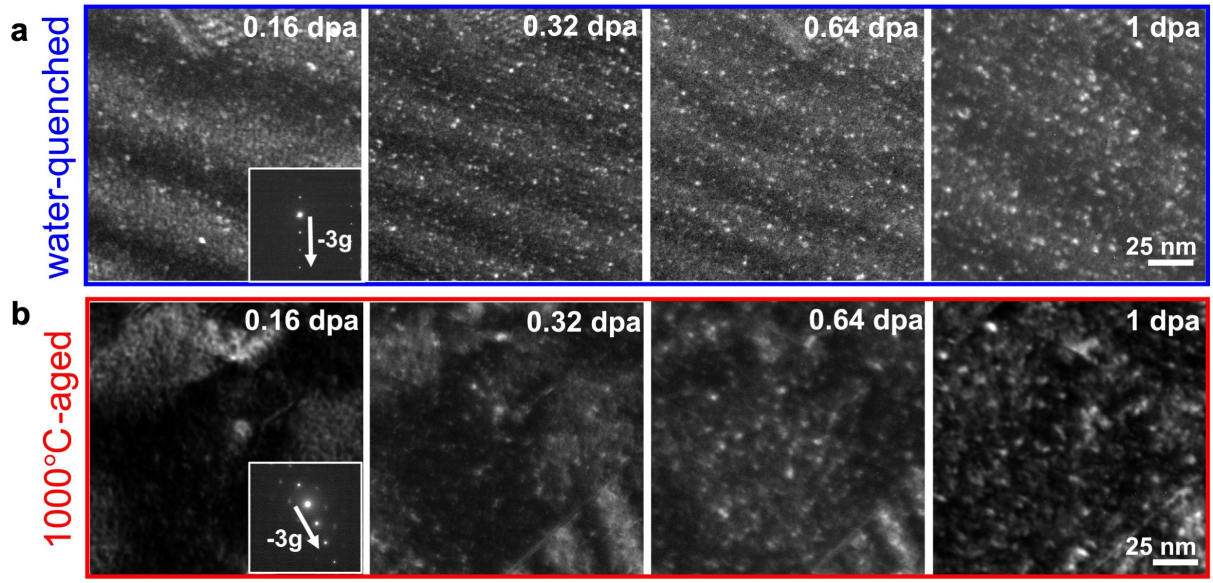


Figure 10: TEM characterization of He+ in situ irradiation. TEM images of (**a**) the water-quenched (RSS), and (**b**) the 1,000 °C-aged (LCO) CrCoNi alloys following various irradiation doses. The irradiation dose progressively increases from 0.16 dpa to 1.0 dpa from left to right. This figure is adapted from Ref. [110].

multi-principal element alloys subjected to irradiation. The destruction and recovery rates of CSRO under irradiation vary significantly with element type and irradiation conditions, highlighting the complexity of predicting long-term radiation behavior. This element-specific evolution underscores a key challenge: establishing predictive models that accurately capture CSRO dynamics during irradiation across diverse alloy systems [116].

Despite these promising advancements, several challenges persist. One critical challenge is the precise experimental characterization of CSRO at atomic scales during dynamic-irradiation processes. Advanced characterization techniques, such as aberration-corrected TEM, APT, synchrotron X-ray diffraction, and neutron scattering, can characterize CSRO. They require high resolution, large data volumes, and careful analysis to distinguish real CSRO effects from experimental noise or artifacts. In-situ irradiation experiments using TEM could help directly observe defect formation and migration as influenced by local chemical environments. Currently, real-time data at atomic resolution remains limited. Furthermore, accurate computational modeling of CSRO evolution under irradiation, particularly at reactor-relevant dose rates and temperatures, requires further refinement and validation through the use of comprehensive experimental data.

In summary, recent advances have established the beneficial effects of CSRO in enhancing radiation resistance through mechanisms involving enhanced defect recombination, suppressed defect cluster growth, and reduced residual defect densities. However, challenges related to precise experimental characterization and predictive modeling of CSRO evolution remain significant. Addressing these challenges through integrated experimental and computational approaches will be crucial for leveraging CSRO as an effective tool in alloy design for improved radiation resistance in future nuclear materials.

4.3 CSRO and hydrogen embrittlement

CSROs have been suggested to deteriorate the hydrogen embrittlement (HE) resistance of austenite steels and CoCrNi CCAs. For example, dynamic strain aging, a typical plastic instability phenomenon characterized by serrated plastic flow in the tensile stress-strain curve, is commonly observed in high-Mn steels as a localized Portevin Le-Chatelier (PLC) band. The origin of this is possibly due to Mn-C CSRO (complexes) [117, 118] and/or the pipe diffusion of C [119]. PLC bands can cause the accumulation of dislocations, therefore facilitating HE in high-Mn steels. Another example is Cr-N interactions in high-nitrogen austenitic steels [120] and Co–Cr–Ni interactions in the CoCrNi alloy [121], which are suggested to be associated with enhanced dislocation planarity. Those subsequently cause microscopic stress concentrations, which play a critical role by causing intergranular and transgranular cracking when hydrogen is present.

On the contrary, several other experiments suggest that CSRO can enhance HE resistance. For example, Liu *et al.* [122] compared the HE of VCoNi medium-entropy alloy with different degrees of CSRO. They found that a higher CSRO degree (achieved by introducing aging treatment and confirmed by aberration-corrected TEM) can significantly trap H within the grain interior, thereby reducing hydrogen segregation at grain boundaries and hindering the diffusion of hydrogen into the alloy's interior. Similarly, the aging heat treatment of Cantor alloy (CrMnFeCoNi) is found to lower the hydrogen diffusion rate and limit the H segregation at GBs and, therefore, prevent detrimental intergranular cracking [123]. Such differences in hydrogen kinetics are suggested to be associated with the formation of NiMn- and Cr-rich nanoclusters at grain boundaries and CSROs within grains.

Recent large-scale atomistic simulations have partially confirmed these beneficial effects [124], revealing a complex interplay between hydrogen and deformation twinning, local chemical ordered (LCO) structures, dislocations, and grain boundaries (GBs) in the Cantor alloy, as summarized in Figure 11. Hydrogen has been found to reduce the SFE and, therefore, promote the deformation twinning. Furthermore, LCO structures act as dynamically trapping sites, forming LCO-H complexes, which show a stronger dislocation-pinning effect than the LCO structures alone. Cr enrichment and Fe depletion found at the GBs can effectively increase GB fracture energy and, therefore, reduce HE sensitivity.

4.4 CSRO and transport properties

Coherent potential approximation (CPA) has demonstrated its ability to predict the physical properties of random solid solutions. However, it is limited to alloys without CSRO due to the inherent single-site approximation. Developed based on CPA, nonlocal CPA (NL-CPA) goes beyond the single-site nature and performs configurational averaging over embedding atomic clusters within an effective medium [125]. The CSRO can be included by embedding a cluster with CSRO explicitly. NL-CPA was first implemented within the KKR formalism and applied to study the effect of CSRO parameters on the electronic structure of the classical alloy, $Cu_{0.5}Zn_{0.5}$ [126, 127]. Another interesting application is in $Fe_{0.5}Pt_{0.5}$ where the spin moment of Pt can be induced by increasing the number of nearby Fe atoms [128]. The implementation of NL-CPA enables an efficient investigation of CSRO on physical properties [129].

The electrical transport property of CCAs is one of the most fundamental physical properties. It encodes the profound impact of the disorder on the electronic structure and Fermi surface. Typically, electrical transport can be greatly suppressed due to disorder-induced electron scattering, resulting in

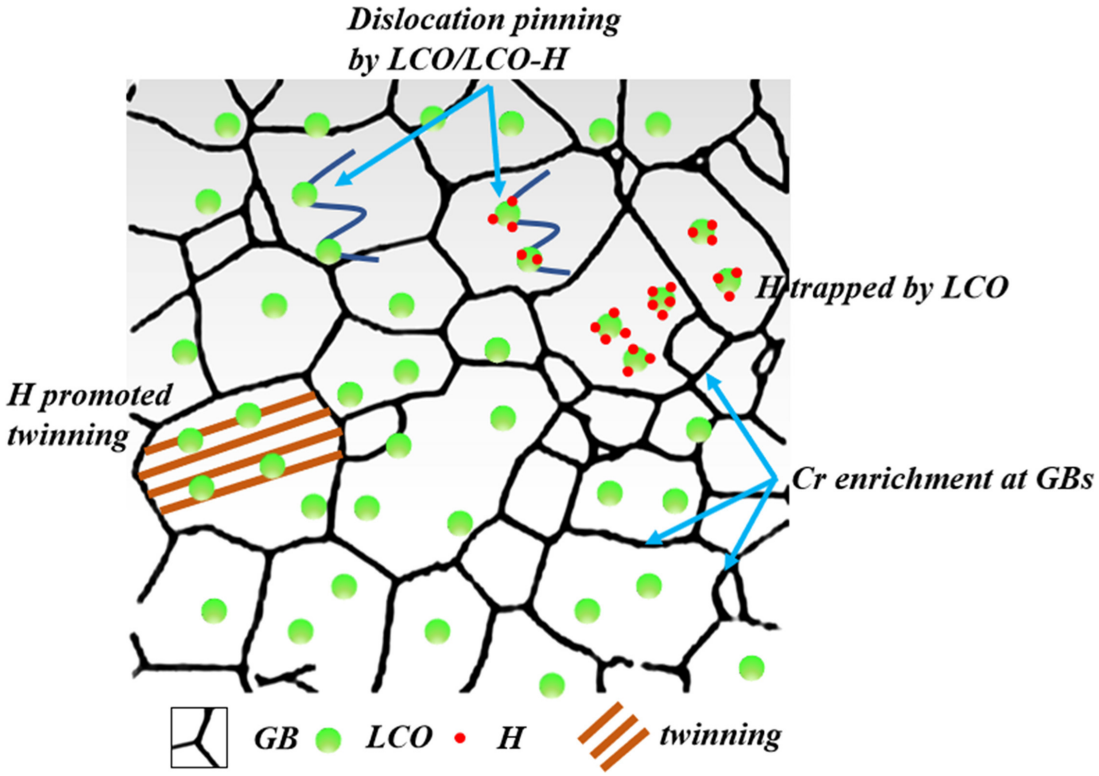


Figure 11: Complex interplay between hydrogen and deformation twinning, local chemical ordered (LCO) structures, dislocations, and grain boundaries (GBs) in the Cantor alloy. This figure is adapted from Ref. [124].

energy dissipation in the form of Joule heat. Thus, the study of electrical transport in CCAs presents an opportunity to understand the effect of disorder on the electronic degree of freedom and the energy dissipation (in the form of heat) via the electron subsystems. Given the vast phase space of CCAs, studying their transport properties can provide valuable insights into efficiently fine-tuning electronic transport by the choice of alloy compositions and varying their concentrations.

To effectively investigate the electrical transport in disordered alloys, Butler reformulated the Kubo-Greenwood (KG) equation within KKR-CPA [130]. This formulation was further implemented in KKR-CPA by Swihart [131], incorporating the vertex correction to evaluate the electrical resistivity of various alloys. We also note that the KG equation was also implemented by Turek *et al.* in the framework of the tight-binding linearized muffin-tin orbital method (TB-LMTO)-CPA [132].

Intuitively, CSRO should increase electrical transport and reduce the electrical resistivity in most scenarios. Employing NL-CPA, Tulip *et al.* [133] explored the CSRO effect on the electron transport in Ag_xPd_{1-x} and found the expected trend – with CSRO, the electrical resistivity reduces. This reduction is also true in Ag_xZn_{1-x} [134] and Cu_xZn_{1-x} [133]. However, there are some exceptions where the residual resistivity increases with CSRO. A well-known example is so-called K-state alloys [135], usually found in Ni, Cr containing alloys [135, 136], such as CoCrNi, Ni25Cr, NiMo, etc. The underlying reason for this bizarre CSRO-enhanced resistivity is attributed to the particular feature of the electronic structure under CSRO, namely, reduced amplitude of d electron hopping in one spin channel between the nearest atomic pair in the presence of CSRO [137].

In addition to the NL-CPA method, the CA-CPA approach [59] provides an alternative ab initio technique within the KKR-CPA framework for studying disordered alloys exhibiting CSRO. This method entails embedding a cluster composed of averaged neighboring atoms, constructed to reflect the CSRO present in the system. The degree of CSRO can be modulated via externally specified order parameters. The resulting averaged cluster can be embedded either in a single-site CPA medium or in a self-consistently derived effective medium that incorporates CSRO effects. The applicability of this method is validated through its implementation for the CuZn body-centered cubic (BCC) solid solution and for AlCrTiV, a quaternary BCC medium-entropy alloy. The CA-CPA method and its combination with the KG formalism for electrical transport are implemented in open-source code MuST [138], enabling the investigation of CSRO effects on electrical conductivity.

Unlike CPA-based effective medium approaches, the LSMS method offers a supercell-based ab initio framework for investigating disordered alloys. Its linear-scaling capability enables efficient first-principles calculations for systems comprising more than 10,000 atoms. Its integration with the KG formalism allows for first-principles calculations of residual resistivity in large-scale systems [139]. LSMS is particularly useful for exploring the influence of short-range ordering in high-entropy alloys, as well as for examining the impact of defects such as stacking faults, dislocations, and other lattice imperfections on electrical resistivity. Furthermore, LSMS can be extended to compute transport properties in noncrystalline systems, including quasicrystals and metallic glasses.

5 Challenges of transforming CSRO into a useful alloy-design tool

We have discussed the effects of CSRO on a variety of physical properties, which provides a diverse and complex prospect for the application of CSRO. It is too early to draw conclusions about the effects

of CSRO on all key physical properties. Nevertheless, for physical properties that most researchers consider to be universally critical, or materials where CSRO has been confirmed to play a dominant role, we expect to transform CSRO into a useful alloy design tool by which CSRO can adjust material properties to achieve design goals. Currently, there are several gaps that prevent us from achieving this goal. We will discuss the challenges that prevent us from achieving this goal by identifying the missing information.

5.1 Experimental challenges in controlling CSRO

The first challenge is how to precisely control CSRO, which can be attributed to three aspects: (i) lack of theoretical guidance; (ii) experimental limitations imposed by the law of diffusion; and (iii) lack of reliable experimental instruments.

Most reports focused on the observation of the microstructure morphology with and without CSRO after heat treatment. These studies may have a qualitative aim to prepare samples with maximal or minimal CSRO. However, few reports mentioned their quantitatively targeted CSRO and methods that allow them to control CSRO accurately using experimental techniques. CSRO is more like an object to be observed rather than precisely controlled. The possible reason could be the lack of a temperature-dependent CSRO as a reference or guiding principle. We need computational methods to provide a clear picture of the evolution of CSRO with temperature and maximize its usage.

CSRO is a combined consequence of kinetics and thermodynamics, making it elusive and hardly controllable. Experimental techniques are limited by diffusion laws. This is reflected in the fact that researchers prefer heat processing in the range of 800-1,200 °C due to the slow kinetics at low temperatures [17]. There are two primary methods for tuning the phases in an alloy system, namely varying temperature and chemical composition. Due to slow kinetics, fine-tuning through temperature usually incurs a time cost in sample preparation [11], which experimentalists generally prefer to avoid. Changing chemical concentration could be ideal, which allows us to shift CSRO at high temperatures.

There is a lack of high-resolution instruments to characterize it. So far, high-resolution TEM cannot reliably characterize large areas to capture CSRO; many atoms are missing in APT, making it unreliable for characterizing CSRO that relies on nearest neighbor information. While neutron scattering can indicate changes in CSRO with peak intensity, this does not correspond uniquely to a structure with the CSRO degree; to obtain the latter, researchers depend significantly on a guessed structure to fit the peaks. Combining machine learning with these experimental instruments suggests a promising pathway to mitigate these issues, as shown by the recent successful examples [140, 10].

5.2 Lack of accurate temperature-dependent CSRO data

The critical role of temperature-dependent CSRO has addressed in understanding experimental observations and designing materials with tunable CSRO [9]. Currently, methods for calculating CSRO include analytical approximations [142] and various Monte Carlo and molecular dynamics simulations, such as simulated annealing, parallel tempering, and the Wang-Landau Monte Carlo method. Different algorithms have their unique advantages and disadvantages. We can utilize them in a combined manner to maximize their benefits in CSRO calculations. Pei and colleagues have used simulated annealing and Wang-Landau algorithms to simulate CoCrNi [9]. The Wang-Landau algorithm can mitigate the issue

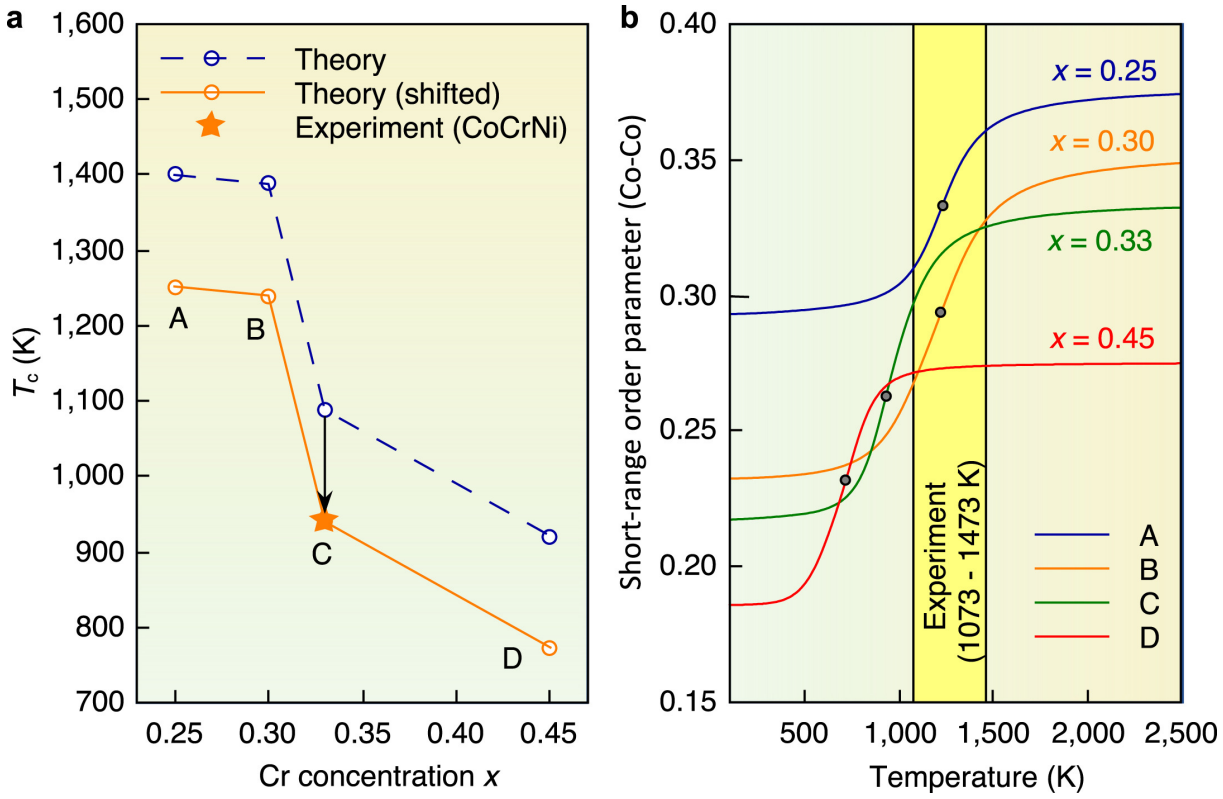


Figure 12: Materials design based on T-dependent CSRO. Tuning the short-range order parameters by varying concentrations enables the design of materials with an idealized degree of CSRO. **a**, Transition temperatures of the short-range ordering are plotted as a function of the Cr concentration. The transition temperatures are identified as the peak locations of the specific heat curves for $Cr_xCo_{(1-x)/2}Ni_{(1-x)/2}$ (x= 25, 30, 33, 45 at.%, represented by A, B, C, and D). The transition temperatures are shifted to the known experimental value for CrCoNi [141] for the alloys. **b**, Temperature-dependent SROs for the four alloys are shown, taking the Co-Co pair as an example. The CSRO curves show that Cr substantially changes the transition temperatures and the magnitudes of the CSRO parameters. These results offer a pathway to maximize the CSRO variance within the common temperature region (yellow region) and test the effects of CSRO on various physical quantities. Alloys A and B are better candidates for studying CSRO effects. This figure is adapted from Ref. [17].

of trapping in high-probability regions, as it does not explicitly include a temperature. The temperature is introduced by the Boltzmann factor, $e^{\beta\Delta E}$. Figure 12 shows an application of their method, where the transition temperatures of a few Co-Cr-Ni alloys were calculated. The phenomenon demonstrated by CSRO can be fine-tuned more effectively by changing chemical concentrations rather than temperature. Modifying CSRO by adjusting chemical concentrations enables the ordering transition to occur at higher temperatures, potentially overcoming sluggish kinetics and making it more advantageous in alloy design. However, this method cannot obtain a configuration that is explicitly specified for a specific temperature and CSRO. To this end, they utilized simulated annealing or parallel tempering for such calculations.

There is still room to improve the flexibility and efficiency in constructing such Hamiltonians or potentials, as well as Monte Carlo algorithms. DFT is accurate but computationally expensive for sufficient sampling in Monte Carlo simulations, which require an impractically long time. The recent work of Pei and colleagues demonstrated that cluster expansion with strain-correction energy can be a promising surrogate model of DFT [17]. ML potentials are efficient in simulations, but training such potentials requires time. We expect that there is a foundation model for empirical potentials that includes all the commonly used chemical elements for structural alloys.

5.3 Lack of practical TTT diagrams

We have discussed the importance of temperature-dependent CSRO with many-body Hamiltonians or potentials, including strain corrections or local distortions. Compared to the temperature-dependent CSRO, the time-temperature-transformation (TTT) diagram is more practical for guiding experiments, as it also indicates the time required to achieve the CSRO. One should be cautious that CSRO is rather short-ranged, with a very short characteristic diffusion length (at the annealing temperature) after the homogenization heat treatment. Therefore, TTT diagrams of CSRO have a very small time scale compared to TTT diagrams for designing experiments. Currently, TTT diagrams are impractical for complex, concentrated alloys. It requires not only accurate Hamiltonians or potentials but also an extremely long time in molecular dynamics (MD) simulations. While MD can be trapped at a local minimum, rare-rate events require impractically long times in real simulations. Current MD simulations are between femtoseconds and nanoseconds. The combination of MD and Monte Carlo (MC) is highly skillful and needs very good judgment of the parameter settings. We need more efficient MD methods or analytical methods that avoid time-consuming MD simulations to achieve this goal.

6 Opportunities and outlook

In the previous section, we discussed a few essential challenges and provided insights into solutions. These challenges and insights also point to new opportunities for future research directions. Based on these challenges, we further our discussion and explore more opportunities.

6.1 CSRO as part of heterogeneous structures

When we can accurately control CSRO, we will have a powerful tool to design high-performance materials for which CSRO play critical roles. Local CSRO can be viewed as one of the heterogeneous

structures, as the atomic or nano-scale morphology of the hierarchical structures. Heterogeneous structures offer greater flexibility for deformation, such as composite structures comprising hard and soft components [109, 15]. It allows for the possibility of both strong and ductile properties to exist in one material. CSRO tuning will join the other existing methods that have become a standard norm in fine-tuning the mechanical properties of metals and alloys. In key challenges, such as overcoming the tradeoff between strength and ductility, CSRO may also play a critical role. This trend is preconditioned on the maturity of techniques in theoretical calculations and experimental characterizations of CSRO. With advances in simulation methods, high-resolution instrumentation, and the increasing involvement of machine learning, we will soon see this goal become increasingly more feasible to realize.

6.2 Additive manufacturing

Additive manufacturing and advanced manufacturing techniques offer new opportunities to design alloys with targeted CSRO degrees in a high-throughput manner since the parameters in the manufacturing process can be well controlled. One way to utilize additive manufacturing is to produce samples with varying cooling rates, as different cooling rates correspond to distinct CSROs, thereby enabling the control of CSRO in different samples [37]. This is an auspicious method compared to existing experiments. Assisted by temperature-dependent CSRO, the experimental design process can be more effective.

In principle, we can manipulate them to design CSRO in alloys flexibly. This can be achieved by controlling key parameters in additive manufacturing, including speed, energy distribution (typically Gaussian or uniform), and temperature distribution, among others. Their relationship may not be straightforward to quantify, and extensive experimental and theoretical efforts are needed to collect relevant data that describe the relationship. We need sufficient and accurate data to tell their correlation. Once their relationships are determined, we can release the full potential of additive manufacturing in controlling CSRO in alloy design.

6.3 Machine-learning potentials

Machine-learning potentials, including neural network potentials, can provide efficient and accurate energy calculations for Monte Carlo and atomistic simulations. The accuracy of neural network potentials is supported by the universal approximation theorem, which states that artificial neural networks can approximate any measurable function to any desired degree of accuracy [143, 144]. The flexibility of ANNs to fit any complex functions makes them particularly suitable for describing complex interatomic interactions. For example, machine-learning potentials like ACE and MTPs exhibit much better performance than classical potentials. However, there is still room to improve their performance further to fully leverage the flexibility and accuracy promised by machine learning. There is a pressing need to develop new machine-learning potentials for materials for which CSRO plays a critical role, and accurate potentials are unavailable. Another exciting direction for machine learning potentials is developing foundation models, or ”universal potentials,” as we pointed out earlier. Once the foundation models are available, the main task remaining is to tailor the models for specific material classes to meet the requirements of individual studies. These potentials will enable the accurate calculation of temperature-dependent physical quantities, such as CSRO and stacking fault energies, which are essential for turning CSRO into a controllable alloy design tool.

Declaration of competing interest

The authors declare that they have no known competing financial interests or personal relationships that could have appeared to influence the work reported in this paper.

Acknowledgments

Z.P. would like to thank the High Performance Computing Group at New York University for their support. The work of P.S. at Ames National Laboratory was supported by the U.S. Department of Energy (DOE), Office of Science, Basic Energy Sciences, Materials Science and Engineering Division. The Ames National Laboratory is operated for the U.S. DOE by Iowa State University under contract DE-AC02-07CH11358. F.K. acknowledges funding through the Heisenberg Programme of the Deutsche Forschungsgemeinschaft (DFG, German Research Foundation) – project number 541649719. Y.L. acknowledges the grant support by National Natural Science Foundation of China (52541015 and 52541016) and National Natural Science Fund for Excellent Young Scientists Fund Program (Overseas). S.M. would like to acknowledge the startup fund from the University of South Carolina, United States. Y.W. would like to acknowledge the grant support by National Science Foundation CSSI-1931525 and CSSI-2103958.

Data availability

No data was used for the research described in the article.

References

[1] Yeh, J.-W. *et al.* Nanostructured high-entropy alloys with multiple principal elements: novel alloy design concepts and outcomes. *Advanced Engineering Materials* **6**, 299–303 (2004).

[2] Cantor, B., Chang, I., Knight, P. & Vincent, A. Microstructural development in equiatomic multicomponent alloys. *Materials Science and Engineering: A* **375**, 213–218 (2004).

[3] Hsu, W.-L., Tsai, C.-W., Yeh, A.-C. & Yeh, J.-W. Clarifying the four core effects of high-entropy materials. *Nature Reviews Chemistry* 1–15 (2024).

[4] Liu, X., Zhang, J. & Pei, Z. Machine learning for high-entropy alloys: Progress, challenges and opportunities. *Progress in Materials Science* 101018 (2022).

[5] Cantor, B. Multicomponent high-entropy cantor alloys. *Progress in Materials Science* 100754 (2020).

[6] Kang, S., Lee, S., Lee, H. & Kang, Y.-M. Manipulating disorder within cathodes of alkali-ion batteries. *Nature Reviews Chemistry* **8**, 587–604 (2024).

[7] He, M., Davids, W. J., Breen, A. J. & Ringer, S. P. Quantifying short-range order using atom probe tomography. *Nature Materials* **23**, 1200–1207 (2024).

[8] Walsh, F., Zhang, M., Ritchie, R. O., Minor, A. M. & Asta, M. Extra electron reflections in concentrated alloys do not necessitate short-range order. *nature materials* **22**, 926–929 (2023).

[9] Pei, Z., Li, R., Gao, M. C. & Stocks, G. M. Statistics of the NiCoCr medium-entropy alloy: Novel aspects of an old puzzle. *npj Computational Materials* **6**, 122 (2020).

[10] Li, Y. *et al.* Machine learning-enabled tomographic imaging of chemical short-range atomic ordering. *Advanced Materials* 2407564 (2024).

[11] Zhang, R. *et al.* Short-range order and its impact on the CrCoNi medium-entropy alloy. *Nature* **581**, 283–287 (2020).

[12] Yin, S. *et al.* Atomistic simulations of dislocation mobility in refractory high-entropy alloys and the effect of chemical short-range order. *Nature communications* **12**, 4873 (2021).

[13] Yin, B., Yoshida, S., Tsuji, N. & Curtin, W. Yield strength and misfit volumes of NiCoCr and implications for short-range-order. *Nature communications* **11**, 2507 (2020).

[14] Li, Q.-J., Sheng, H. & Ma, E. Strengthening in multi-principal element alloys with local-chemical-order roughened dislocation pathways. *Nature communications* **10**, 3563 (2019).

[15] Chen, S. *et al.* Simultaneously enhancing the ultimate strength and ductility of high-entropy alloys via short-range ordering. *Nature communications* **12**, 4953 (2021).

[16] Ferrari, A., Körmann, F., Asta, M. & Neugebauer, J. Simulating short-range order in compositionally complex materials. *Nature Computational Science* **3**, 221–229 (2023).

[17] Pei, Z., Zhang, X., Eisenbach, M. & Liaw, P. K. Rigorous computation of short-range order unifies its controversial effects in complex concentrated alloys. *Acta Materialia* 120713 (2025).

[18] Ding, J., Yu, Q., Asta, M. & Ritchie, R. O. Tunable stacking fault energies by tailoring local chemical order in CrCoNi medium-entropy alloys. *Proceedings of the National Academy of Sciences* **115**, 8919–8924 (2018).

[19] Yoshida, S., Bhattacharjee, T., Bai, Y. & Tsuji, N. Friction stress and hall-petch relationship in CoCrNi equi-atomic medium entropy alloy processed by severe plastic deformation and subsequent annealing. *Scripta Materialia* **134**, 33–36 (2017).

[20] Zhao, Y. *et al.* Heterogeneous precipitation behavior and stacking-fault-mediated deformation in a CoCrNi-based medium-entropy alloy. *Acta Materialia* **138**, 72–82 (2017).

[21] Uzer, B. *et al.* On the mechanical response and microstructure evolution of NiCoCr single crystalline medium entropy alloys. *Materials Research Letters* **6**, 442–449 (2018).

[22] Sohn, S. S. *et al.* Ultrastrong medium-entropy single-phase alloys designed via severe lattice distortion. *Advanced Materials* **31**, 1807142 (2019).

[23] Praveen, S., Bae, J. W., Asghari-Rad, P., Park, J. M. & Kim, H. S. Ultra-high tensile strength nanocrystalline CoCrNi equi-atomic medium entropy alloy processed by high-pressure torsion. *Materials Science and Engineering: A* **735**, 394–397 (2018).

[24] Pei, Z., Eisenbach, M., Mu, S. & Stocks, G. M. Error controlling of the combined cluster-expansion and Wang–Landau Monte-Carlo method and its application to FeCo. *Computer Physics Communications* **235**, 95–101 (2019).

[25] Santodonato, L. J., Liaw, P. K., Unocic, R. R., Bei, H. & Morris, J. R. Predictive multiphase evolution in Al-containing high-entropy alloys. *Nature communications* **9**, 4520 (2018).

[26] Khan, S. N., Staunton, J. B. & Stocks, G. M. Statistical physics of multicomponent alloys using KKR-CPA. *Phys. Rev. B* **93**, 054206 (2016).

[27] Porter, D. & Easterling, K. *Phase Transformations in Metals and Alloys, Third Edition (Revised Reprint)* (Taylor & Francis, 1992).

[28] Rahaman, M., Johansson, B. & Ruban, A. First-principles study of atomic ordering in FCC Ni-Cr alloys. *Physical Review B* **89**, 064103 (2014).

[29] Cowley, J. An approximate theory of order in alloys. *Physical Review* **77**, 669–675 (1950).

[30] Clapp, P. & Moss, S. Correlation functions of disordered binary alloys. I. *Physical Review* **142**, 418–427 (1966).

[31] Egami, T. & Billinge, S. *Underneath the Bragg Peaks: Structural Analysis of Complex Materials* (Pergamon, 2012), 2nd edn.

[32] Liu, X. *et al.* Revealing nanostructures in high-entropy alloys via machine-learning accelerated scalable Monte Carlo simulation. *npj Computational Materials* **11**, 267 (2025).

[33] Krivoglaz, M. A. & Smirnov, A. A. The theory of order-disorder in alloys. *(No Title)* (1964).

[34] Chen, X. *et al.* Direct observation of chemical short-range order in a medium-entropy alloy. *Nature* **592**, 712–716 (2021).

[35] Di Russo, E. *et al.* Order and disorder at the atomic scale: Microscopy applied to semiconductors. *Reviews of Modern Physics* **97**, 025006 (2025).

[36] Hsiao, H.-W. *et al.* Data-driven electron-diffraction approach reveals local short-range ordering in CrCoNi with ordering effects. *Nature communications* **13**, 6651 (2022).

[37] Han, Y. *et al.* Ubiquitous short-range order in multi-principal element alloys. *Nature Communications* **15**, 6486 (2024).

[38] Seol, J. B. *et al.* Mechanically derived short-range order and its impact on the multi-principal-element alloys. *Nature communications* **13**, 6766 (2022).

[39] Li, L. *et al.* Atomic-scale probing of short-range order and its impact on electrochemical properties in cation-disordered oxide cathodes. *Nature Communications* **14**, 7448 (2023).

[40] Zhou, L. *et al.* Atomic-scale evidence of chemical short-range order in CrCoNi medium-entropy alloy. *Acta Materialia* **224**, 117490 (2022).

[41] Walsh, F., Zhang, M., Ritchie, R. O., Asta, M. & Minor, A. M. Multiple origins of extra electron diffractions in FCC metals. *Science Advances* **10**, eadn9673 (2024).

[42] Owen, L., Stone, H. & Playford, H. The assessment of local lattice strains in alloys using total scattering. *Acta Materialia* **170**, 38–49 (2019).

[43] Fantin, A. *et al.* Short-range chemical order and local lattice distortion in a compositionally complex alloy. *Acta Materialia* **193**, 329–337 (2020).

[44] Dove, M. T., Tucker, M. G. & Keen, D. A. Neutron total scattering method: simultaneous determination of long-range and short-range order in disordered materials. *European Journal of Mineralogy* **14**, 331–348 (2002).

[45] Owen, L., Playford, H., Stone, H. & Tucker, M. A new approach to the analysis of short-range order in alloys using total scattering. *Acta Materialia* **115**, 155–166 (2016).

[46] Walker, C. & Keating, D. Neutron diffraction study of short-range order in β-CuZn. *Physical Review* **130**, 1726 (1963).

[47] Cenedese, P., Bley, F. & Lefebvre, S. Diffuse scattering in disordered ternary alloys: neutron measurements of local order in a stainless steel Fe0. 56Cr0. 21Ni0. 23. *Foundations of Crystallography* **40**, 228–240 (1984).

[48] Menshikov, A., Dimitrov, C. & Teplykh, A. Local atomic redistribution under irradiation in γ–NiFeCr alloys. *Journal de Physique III* **7**, 1899–1908 (1997).

[49] Zhang, F. *et al.* Local structure and short-range order in a NiCoCr solid solution alloy. *Physical review letters* **118**, 205501 (2017).

[50] Li, Y. *et al.* Machine learning enhanced atom probe tomography analysis. *Progress in Materials Science* **156**, 101561 (2026). URL `https://www.sciencedirect.com/science/article/pii/S0079642525001392`.

[51] Li, Y. *et al.* Quantitative three-dimensional imaging of chemical short-range order via machine learning enhanced atom probe tomography. *Nature Communications* **14**, 7410 (2023).

[52] Li, Y., Nutor, R. K. & Gault, B. L12-type chemical short-range ordering in compositionally complex alloys. *Journal of Materials Science & Technology* **250**, 188–196 (2026). URL `https://www.sciencedirect.com/science/article/pii/S100503022500739X`.

[53] Sanchez, J. M., Ducastelle, F. & Gratias, D. Generalized cluster description of multicomponent systems. *Physica A: Statistical Mechanics and its Applications* **128**, 334–350 (1984).

[54] Drautz, R. Atomic cluster expansion for accurate and transferable interatomic potentials. *Physical Review B* **99**, 014104 (2019).

[55] Shapeev, A. V. Moment tensor potentials: A class of systematically improvable interatomic potentials. *Multiscale Modeling & Simulation* **14**, 1153–1173 (2016).

[56] Bartók, A. P., Payne, M. C., Kondor, R. & Csányi, G. Gaussian approximation potentials: The accuracy of quantum mechanics, without the electrons. *Physical review letters* **104**, 136403 (2010).

[57] Korringa, J. On the calculation of the energy of a bloch wave in a metal. *Physica* **13**, 392–400 (1947). URL https://www.sciencedirect.com/science/article/pii/003189144790013X.

[58] Kohn, W. & Rostoker, N. Solution of the Schrödinger equation in periodic lattices with an application to metallic lithium. *Phys. Rev.* **94**, 1111–1120 (1954). URL https://link.aps.org/doi/10.1103/PhysRev.94.1111.

[59] Raghuraman, V., Wang, Y. & Widom, M. Averaged cluster approach to including chemical short-range order in KKR-CPA. *Phys. Rev. B* **102**, 054207 (2020).

[60] Wang, Y. *et al.* Order-n multiple scattering approach to electronic structure calculations. *Phys. Rev. Lett.* **75**, 2867–2870 (1995).

[61] Yin, J., Pei, Z. & Gao, M. C. Neural network-based order parameter for phase transitions and its applications in high-entropy alloys. *Nature Computational Science* **1**, 686–693 (2021).

[62] Ebert, H., Mankovsky, S., Ködderitzsch, D. & Kelly, P. J. Ab initio calculation of the Gilbert damping parameter via the linear response formalism. *Phys. Rev. Lett.* **107**, 066603 (2011).

[63] Shapeev, A. Accurate representation of formation energies of crystalline alloys with many components. *Computational Materials Science* **139**, 26–30 (2017).

[64] Singh, P., Smirnov, A. V. & Johnson, D. D. Atomic short-range order and incipient long-range order in high-entropy alloys. *Physical Review B* **91**, 224204 (2015).

[65] Singh, P., Smirnov, A. V. & Johnson, D. D. Ta-nb-mo-w refractory high-entropy alloys: anomalous ordering behavior and its intriguing electronic origin. *Physical Review Materials* **2**, 055004 (2018).

[66] Singh, P. *et al.* Tuning phase-stability and short-range order through Al-doping in (CoCrFeMn)_100-xAl_x high entropy alloys. *Physical Review Materials* **3**, 075002 (2019).

[67] Singh, P., Smirnov, A. V., Alam, A. & Johnson, D. D. First-principles prediction of incipient order in arbitrary high-entropy alloys: exemplified in Ti0.25CrFeNiAl_x. *Acta Materialia* **189**, 248–254 (2020).

[68] Singh, P. *et al.* Martensitic transformation in Fe_xMn_{80}-x$Co_{10}Cr_{10}$ high-entropy alloy. *Physical Review Letters* **127**, 115704 (2021).

[69] Singh, P. & Johnson, D. D. Designing order-disorder transformation in high-entropy ferritic steels. *Journal of Materials Research* **9** (2021).

[70] Staunton, J. B., Johnson, D. D. & Pinski, F. J. Compositional short-range ordering in metallic alloys: Band-filling, charge-transfer, and size effects from a first-principles all-electron Landau-type theory. *Physical Review B* **50**, 1450 (1994).

[71] Johnson, D. D., Staunton, J. B. & Pinski, F. J. First-principles all-electron theory of atomic short-range ordering in metallic alloys: D0_22- versus l1_2-like correlations. *Physical Review B* **50**, 1473 (1994).

[72] Johnson, D. D. Computation of diffuse intensities in alloys. In Kaufmann, E. N. (ed.) *Characterization of Materials*, 1–31 (John Wiley and Sons, Inc., 2012).

[73] Staunton, J. B., Johnson, D. D. & Pinski, F. J. Theory of compositional and magnetic correlations in alloys: Interpretation of a diffuse neutron-scattering experiment on an iron-vanadium single crystal. *Physical Review Letters* **65**, 1259 (1990).

[74] Györffy, B. L. & Stocks, G. M. Concentration waves and Fermi surfaces in random metallic alloys. *Physical Review Letters* **50**, 374 (1983).

[75] Györffy, B. L. *et al.* Alloy Phase Stability. In Stocks, G. M. & Gonis, A. (eds.) *Alloy Phase Stability*, 421 (Kluwer, Dordrecht, 1989).

[76] Picak, S. *et al.* Orientation dependence of the effect of short-range ordering on the plastic deformation of a medium entropy alloy. *Materials Science & Engineering A* **888**, 145309 (2023).

[77] Körmann, F., Ruban, A. V. & Sluiter, M. H. F. Long-ranged interactions in BCC NbMoTaW high-entropy alloys. *Materials Research Letters* **5**, 35–40 (2017).

[78] Zhang, F. X. *et al.* Local structure and short-range order in a NiCoCr solid solution alloy. *Phys. Rev. Lett.* **118**, 205501 (2017).

[79] Naghdi, A., Domínguez-Gutiérrez, F. J., Huo, W. Y., Karimi, K. & Papanikolaou, S. Dynamic nanoindentation and short-range order in equiatomic NiCoCr medium-entropy alloy lead to novel density wave ordering. *Phys. Rev. Lett.* **132**, 116101 (2024).

[80] Robarts, H. C. *et al.* Extreme Fermi surface smearing in a maximally disordered concentrated solid solution. *Phys. Rev. Lett.* **124**, 046402 (2020).

[81] Banerjee, T., Sharma, A., Picak, S., Lattemann, M. & Singh, P. An atomistic study connecting underlying dislocation behavior with superior mechanical properties of NiCoCr medium entropy alloy. *Materials Today Communications* **44**, 112065 (2025).

[82] Morris, W., Johnson, D. D. & Singh, P. Accurate prediction of chemical short-range order and its effect on thermodynamic, structural, and electronic properties of disordered alloys: Exemplified in Cu3Au. *Materials Today Communications* **35**, 106214 (2023).

[83] Xu, B. *et al.* Mechanism of sluggish diffusion under rough energy landscape. *Cell Reports Physical Science* **4** (2023).

[84] Xing, B., Rupert, T. J., Pan, X. & Cao, P. Neural network kinetics for exploring diffusion multiplicity and chemical ordering in compositionally complex materials. *Nature Communications* **15**, 3879 (2024).

[85] Zhang, Y.-W. *et al.* Roadmap for the development of machine learning-based interatomic potentials. *Modelling and Simulation in Materials Science and Engineering* **33**, 023301 (2025).

[86] Behler, J. & Parrinello, M. Generalized neural-network representation of high-dimensional potential-energy surfaces. *Physical review letters* **98**, 146401 (2007).

[87] Kostiuchenko, T., Körmann, F., Neugebauer, J. & Shapeev, A. Impact of lattice relaxations on phase transitions in a high-entropy alloy studied by machine-learning potentials. *npj Computational Materials* **5**, 55 (2019).

[88] Ghosh, S., Sotskov, V., Shapeev, A. V., Neugebauer, J. & Körmann, F. Short-range order and phase stability of CrCoNi explored with machine learning potentials. *Physical Review Materials* **6**, 113804 (2022).

[89] Ghosh, S., Ueltzen, K., George, J., Neugebauer, J. & Körmann, F. Chemical ordering and magnetism in face-centered cubic CrCoNi alloy. *npj Computational Materials* **10**, 284 (2024).

[90] Sheriff, K., Cao, Y., Smidt, T. & Freitas, R. Quantifying chemical short-range order in metallic alloys. *Proceedings of the National Academy of Sciences* **121**, e2322962121 (2024).

[91] Woodgate, C. D., Hedlund, D., Lewis, L. & Staunton, J. B. Interplay between magnetism and short-range order in medium-and high-entropy alloys: CrCoNi, CrFeCoNi, and CrMnFeCoNi. *Physical Review Materials* **7**, 053801 (2023).

[92] Kostiuchenko, T. S., Shapeev, A. V. & Novikov, I. S. Interatomic interaction models for magnetic materials: Recent advances. *Chinese Physics Letters* (2024).

[93] Rinaldi, M., Mrovec, M., Bochkarev, A., Lysogorskiy, Y. & Drautz, R. Non-collinear magnetic atomic cluster expansion for iron. *npj Computational Materials* **10**, 12 (2024).

[94] Novikov, I., Grabowski, B., Körmann, F. & Shapeev, A. Magnetic moment tensor potentials for collinear spin-polarized materials reproduce different magnetic states of BCC Fe. *npj Computational Materials* **8**, 13 (2022).

[95] Bienvenu, B. *et al.* Development of an atomic cluster expansion potential for iron and its oxides. *arXiv preprint arXiv:2407.13903* (2024).

[96] Shenoy, L. *et al.* Collinear-spin machine learned interatomic potential for Fe 7 Cr 2 Ni alloy. *Physical Review Materials* **8**, 033804 (2024).

[97] Borges, P. P., Ritchie, R. O. & Asta, M. Chemical trends favoring interstitial cluster formation in BCC high-entropy alloys from first-principles calculations. *Acta Materialia* 121091 (2025).

[98] Müller, Y. L. & Natarajan, A. R. Constructing multicomponent cluster expansions with machine-learning and chemical embedding. *npj Computational Materials* **11**, 60 (2025).

[99] Rigamonti, S., Troppenz, M., Kuban, M., Hübner, A. & Draxl, C. Cell: a Python package for cluster expansion with a focus on complex alloys. *npj Computational Materials* **10**, 195 (2024).

[100] Kanzaki, H. Point defects in face-centred cubic lattice—I distortion around defects. *Journal of Physics and Chemistry of Solids* **2**, 24–36 (1957).

[101] Antillon, E., Woodward, C., Rao, S., Akdim, B. & Parthasarathy, T. Chemical short range order strengthening in a model FCC high entropy alloy. *Acta Materialia* **190**, 29–42 (2020).

[102] Antillon, E., Woodward, C., Rao, S. & Akdim, B. Chemical short range order strengthening in BCC complex concentrated alloys. *Acta Materialia* **215**, 117012 (2021).

[103] Nag, S. & Curtin, W. A. Solute-strengthening in metal alloys with short-range order. *Acta Materialia* **263**, 119472 (2024).

[104] You, D. *et al.* Short-range ordering mechanics in FCC materials. *International Journal of Plasticity* **174**, 103919 (2024).

[105] Pei, J.-M. *et al.* Review: chemical short-range order in high-entropy alloys and its effect on mechanical properties. *Journal of Materials Science* (2025). URL `https://doi.org/10.1007/s10853-025-11991-3`.

[106] Zhao, B., Song, H. & An, M. The dual role of short-range order: A critical temperature switch between strengthening and weakening in high-entropy alloys. *Journal of Materials Research and Technology* **41**, 90–99 (2026).

[107] Ma, E. & Liu, C. Chemical inhomogeneities in high-entropy alloys help mitigate the strength-ductility trade-off. *Progress in Materials Science* 101252 (2024).

[108] Sun, L. *et al.* Local chemical order enables an ultrastrong and ductile high-entropy alloy in a cryogenic environment. *Science Advances* **10**, eadq6398 (2024).

[109] Yan, Y.-Q. *et al.* Ductilization of 2.6-GPa alloys via short-range ordered interfaces and supranano precipitates. *Science* **387**, 401–406 (2025).

[110] Zhang, Z. *et al.* Effect of local chemical order on the irradiation-induced defect evolution in Cr-CoNi medium-entropy alloy. *Proceedings of the National Academy of Sciences* **120**, e2218673120 (2023).

[111] Cao, P. How does short-range order impact defect kinetics in irradiated multiprincipal element alloys? *Accounts of Materials Research* **2**, 71–74 (2021).

[112] Su, Z. *et al.* Enhancing the radiation tolerance of high-entropy alloys via solute-promoted chemical heterogeneities. *Acta Materialia* **245**, 118662 (2023).

[113] Curtis, N. *et al.* Local chemical ordering of a neutron-irradiated crfemnni compositionally complex alloy. *Acta Materialia* 120752 (2025).

[114] Mo, Y., Liang, Y., Guo, W., Tian, Y. & Wan, Q. Atomistic simulation of chemical short-range order on the irradiation resistance of HfNbTaTiZr high entropy alloy. *International Journal of Plasticity* **183**, 104155 (2024).

[115] Arkoub, H. & Jin, M. Impact of chemical short-range order on radiation damage in Fe-Ni-Cr alloys. *Scripta Materialia* **229**, 115373 (2023).

[116] Zhou, Y. *et al.* Element-dependent evolution of chemical short-range ordering tendency of NiCoFeCrMn under irradiation. *International Journal of Plasticity* **171**, 103768 (2023).

[117] Koyama, M., Sawaguchi, T. & Tsuzaki, K. Overview of dynamic strain aging and associated phenomena in Fe–Mn–C austenitic steels. *ISIJ International* **58**, 1383–1395 (2018).

[118] Koyama, M., Sawaguchi, T., Lee, T., Lee, C. S. & Tsuzaki, K. Work hardening associated with ϵ-martensitic transformation, deformation twinning and dynamic strain aging in Fe–17Mn–0.6C and Fe–17Mn–0.8C twip steels. *Materials Science and Engineering: A* **528**, 7310–7316 (2011).

[119] Oh, S.-K. *et al.* The mechanism of dynamic strain aging for type a serrations in tensile flow curves of Fe-18Mn-0.55C (wt.%) twinning-induced plasticity steel. *Acta Materialia* **188**, 366–375 (2020).

[120] Koyama, M., Habib, K., Masumura, T., Tsuchiyama, T. & Noguchi, H. Gaseous hydrogen embrittlement of a Ni-free austenitic stainless steel containing 1 mass% nitrogen: Effects of nitrogen-enhanced dislocation planarity. *International Journal of Hydrogen Energy* **45**, 10209–10218 (2020).

[121] Zhang, R. *et al.* Short-range order and its impact on the CrCoNi medium-entropy alloy. *Nature* **581**, 283–287 (2020).

[122] Liu, G.-D. *et al.* Effect of short-range order on hydrogen-induced cracking of VCoNi medium entropy alloy. *Materials Characterization* **217**, 114329 (2024).

[123] Wu, P. *et al.* Ordering-facilitated lower hydrogen embrittlement sensitivity in a prototype high-entropy alloy. *Materials Characterization* **218**, 114473 (2024).

[124] Zhou, X.-Y. *et al.* Enhanced hydrogen embrittlement resistance of FeCoNiCrMn multi-principal element alloys via local chemical ordering and grain boundary segregation. *Acta Materialia* 121209 (2025).

[125] Jarrell, M. & Krishnamurthy, H. R. Systematic and causal corrections to the coherent potential approximation. *Phys. Rev. B* **63**, 125102 (2001).

[126] Rowlands, D. A., Staunton, J. B., Györffy, B. L., Bruno, E. & Ginatempo, B. Effects of short-range order on the electronic structure of disordered metallic systems. *Phys. Rev. B* **72**, 045101 (2005).

[127] Rowlands, D. A., Ernst, A., Györffy, B. & Staunton, J. B. Density functional theory for disordered alloys with short-range order: Systematic inclusion of charge-correlation effects. *Phys. Rev. B* **73**, 165122 (2006).

[128] Ködderitzsch, D., Ebert, H., Rowlands, D. & Ernst, A. Relativistic formulation of the Korringa–Kohn–Rostoker nonlocal coherent-potential approximation. *New J. Phys.* **9**, 81 (2007).

[129] Rowlands, D. A. Short-range correlations in disordered systems: nonlocal coherent-potential approximation. *Rep. Prog. Phys.* **72**, 086501 (2009).

[130] Butler, W. H. Theory of electronic transport in random alloys: Korringa-Kohn-Rostoker coherent-potential approximation. *Phys. Rev. B* **31**, 3260 (1985).

[131] Swihart, J. C., Butler, W. H., Stocks, G. M., Nicholson, D. & Ward, R. First-principles calculation of the residual electrical resistivity of random alloys. *Phys. Rev. Lett.* **57**, 1181 (1986).

[132] Turek, I., Kudrnovskỳ, J., Drchal, V., Szunyogh, L. & Weinberger, P. Interatomic electron transport by semiempirical and ab initio tight-binding approaches. *Phys. Rev. B* **65**, 125101 (2002).

[133] Tulip, P., Staunton, J. B., Lowitzer, S., Koedderitzsch, D. & Ebert, H. Theory of electronic transport in random alloys with short-range order: Korringa-Kohn-Rostoker nonlocal coherent potential approximation. *Phys. Rev. B* **77**, 165116 (2008).

[134] Migschitz, M., Garlipp, W. & Pfeiler, W. Short-range order kinetics in α-agzn for various states of post-deformation defect annealing after cold-rolling. *Acta materialia* **44**, 2831–2838 (1996).

[135] Thomas, H. Über widerstandslegierungen. *Zeitschrift für Physik* **129**, 219–232 (1951).

[136] Nicholson, D. & Brown, R. Electrical resistivity of Ni 0.8 Mo 0.2: Explanation of anomalous behavior in short-range ordered alloys. *Phys. Rev. Lett.* **70**, 3311 (1993).

[137] Lowitzer, S. *et al.* An ab initio investigation of how residual resistivity can decrease when an alloy is deformed. *Euro. Lett.* **92**, 37009 (2010).

[138] Must project. `https://github.com/mstsuite/MuST`.

[139] Raghuraman, V., Widom, M., Eisenbach, M. & Wang, Y. First-principles residual resistivity using a locally self-consistent multiple scattering method. *Phys. Rev. B* **109**, 104204 (2024). URL `https://link.aps.org/doi/10.1103/PhysRevB.109.104204`.

[140] Kalinin, S. V. *et al.* Machine learning in scanning transmission electron microscopy. *Nature Reviews Methods Primers* **2**, 11 (2022).

[141] Jin, K. *et al.* Thermophysical properties of ni-containing single-phase concentrated solid solution alloys. *Materials & Design* **117**, 185–192 (2017).

[142] Rao, Y. & Curtin, W. Analytical models of short-range order in FCC and BCC alloys. *Acta Materialia* **226**, 117621 (2022).

[143] Hornik, K., Stinchcombe, M. & White, H. Multilayer feedforward networks are universal approximators. *Neural networks* **2**, 359–366 (1989).

[144] Cybenko, G. Approximation by superpositions of a sigmoidal function. *Mathematics of control, signals and systems* **2**, 303–314 (1989).